AGU PUBLICATIONS

JGR

Journal of Geophysical Research: Solid Earth

RESEARCH ARTICLE
10.1002/2013JB010476

Key Points:
- Thin oceanic crust inferred in the Seine Abyssal Plain
- New classification of the geological domains off SW Iberia
- New geodynamic reconstruction of the Central Atlantic-Western Tethys system

Supporting Information:
- Readme
- Figure S1a
- Figure S1b
- Figure S1c
- Figure S1d
- Figure S1e
- Figure S2

Correspondence to:
S. Martínez-Loriente,
smartinez@icm.csic.es

Citation:
Martínez-Loriente, S., V. Sallarès, E. Gràcia, R. Bartolome, J. J. Dañobeitia, and N. Zitellini (2014), Seismic and gravity constraints on the nature of the basement in the Africa-Eurasia plate boundary: New insights for the geodynamic evolution of the SW Iberian margin, *J. Geophys. Res. Solid Earth*, *119*, 127–149, doi:10.1002/2013JB010476.

Received 28 JUN 2013
Accepted 21 DEC 2013
Accepted article online 28 DEC 2013
Published online 27 JAN 2014

Seismic and gravity constraints on the nature of the basement in the Africa-Eurasia plate boundary: New insights for the geodynamic evolution of the SW Iberian margin

Sara Martínez-Loriente[1], Valentí Sallarès[1], Eulàlia Gràcia[1], Rafael Bartolome[1], Juan José Dañobeitia[2], and Nevio Zitellini[3]

[1]B-CSI, Institut de Ciències del Mar, CSIC, Barcelona, Spain, [2]Unidad de Tecnología Marina, CSIC, Barcelona, Spain, [3]Istituto Scienze Marine, CNR, Sezione Geologia Marina, Bologna, Italy

Abstract We present a new classification of geological domains at the Africa-Eurasia plate boundary off SW Iberia, together with a regional geodynamic reconstruction spanning from the Mesozoic extension to the Neogene-to-present-day convergence. It is based on seismic velocity and density models along a new transect running from the Horseshoe to the Seine abyssal plains, which is combined with previously available geophysical models from the region. The basement velocity structure at the Seine Abyssal Plain indicates the presence of a highly heterogeneous, thin oceanic crust with local high-velocity anomalies possibly representing zones related to the presence of ultramafic rocks. The integration of this model with previous ones reveals the presence of three oceanic domains offshore SW Iberia: (1) the Seine Abyssal Plain domain, generated during the first stages of slow seafloor spreading in the NE Central Atlantic (Early Jurassic); (2) the Gulf of Cadiz domain, made of oceanic crust generated in the Alpine-Tethys spreading system between Iberia and Africa, which was coeval with the formation of the Seine Abyssal Plain domain and lasted up to the North Atlantic continental breakup (Late Jurassic); and (3) the Gorringe Bank domain, made of exhumed mantle rocks, which formed during the first stages of North Atlantic opening. Our models suggest that the Seine Abyssal Plain and Gulf of Cadiz domains are separated by the Lineament South strike-slip fault, whereas the Gulf of Cadiz and Gorringe Bank domains appear to be limited by a deep thrust fault located at the center of the Horseshoe Abyssal Plain.

1. Introduction

The Atlantic segment of the Eurasia-Africa plate boundary, the so-called Azores-Gibraltar fracture zone, shows a changing tectonic behavior (i.e., extensional, transcurrent, and compressional) from West to East. On its eastern end, at the SW Iberian margin, the system is dominated by compression related to the NW-SE trending convergence (3.8–5.6 mm/yr) [*Nocquet and Calais*, 2004; *DeMets et al.*, 2010] between the two plates. This setting is at the origin of the moderate magnitude seismic activity ($M_w < 6.0$) that occurs in the region [e.g., *Stich et al.*, 2006] and of the large-magnitude historical and instrumental earthquakes, such as the 1755 Lisbon (estimated $M_w \geq 8.5$) [e.g., *Buforn et al.*, 2004, *Johnston*, 1996] and the 1969 Horseshoe ($M_w \sim 8.0$) [e.g., *Fukao*, 1973] earthquakes. In addition, the area is supposed to host one of the oldest oceanic lithospheres currently preserved on Earth [e.g., *Sartori et al.*, 1994; *Rovere et al.*, 2004; *Sallarès et al.*, 2011; *Martínez-Loriente et al.*, 2013], and consequently, the nature and distribution of the basement in SW Iberia has been a matter of enduring debate for decades [e.g., *Purdy*, 1975; *Sartori et al.*, 1994; *Tortella et al.*, 1997; *Hayward et al.*, 1999; *Gràcia et al.*, 2003b; *Thiebot and Gutscher*, 2006; *Jiménez-Munt et al.*, 2010; *Sallarès et al.*, 2013]. Defining and characterizing the basement affinity of the crustal domains in the SW Iberian margin is of paramount importance as it is directly related not only to the initial stages of geodynamic evolution of the Central and North Atlantic but also to the generation of earthquakes and potential subsequent tsunamis in the area.

The basement of the SW Iberian margin is a product of the complex geodynamic history, kinematics, and tectonic evolution of this area that has resulted from the relative motion of the African, Eurasian, and North American plates between the Jurassic and present times [e.g., *Srivastava et al.*, 1990; *Tucholke et al.*, 2007; *Schettino and Turco*, 2009]. The area has been the site of multiple experiments including deep-sea drilling [e.g., *Hayes et al.*, 1972; *Ryan et al.*, 1973], dredging [e.g., *Malod and Mougenot*, 1979], deep-sea submersible

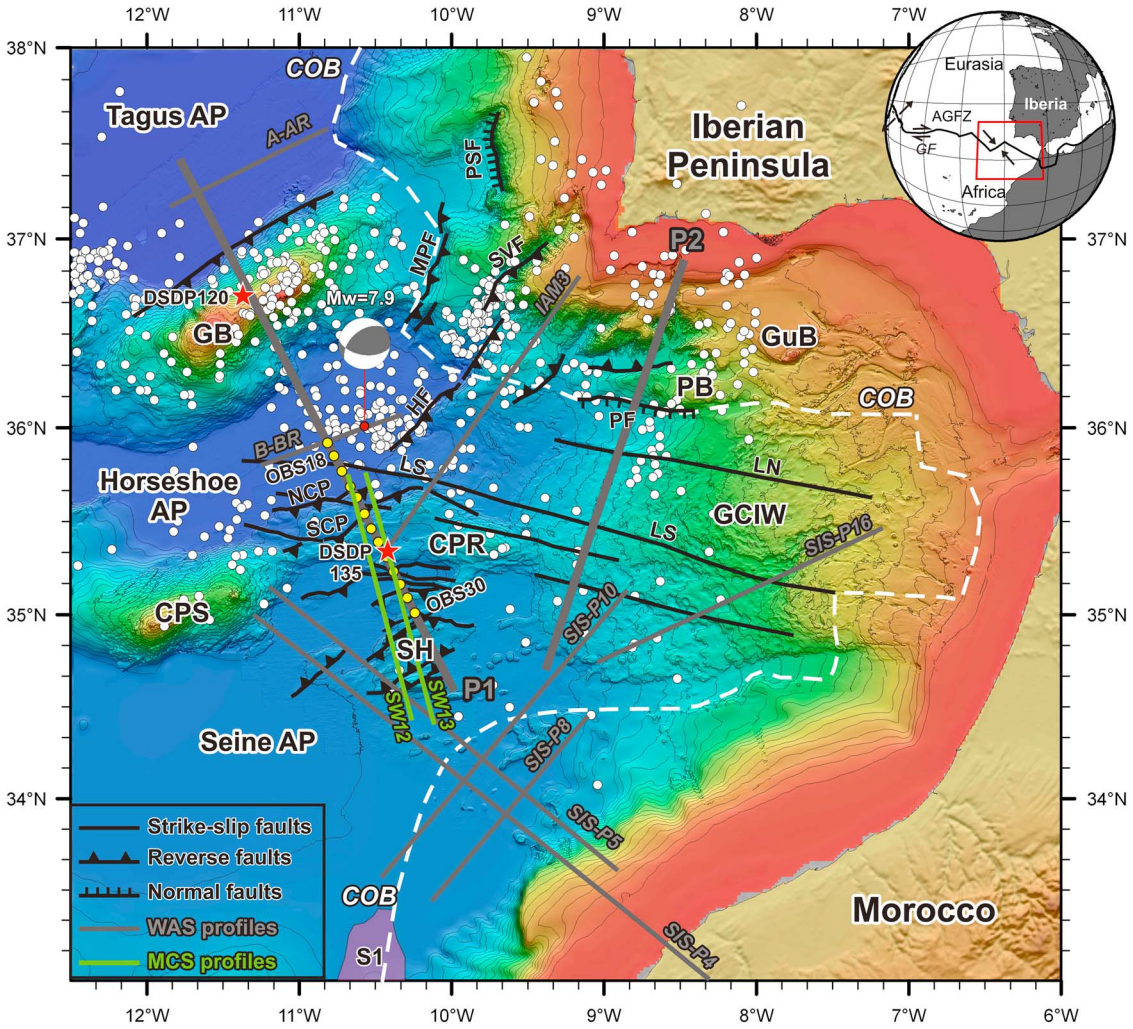

Figure 1. Bathymetric map of the SW Iberian and NW African margins. The multibeam bathymetry merges the SWIM compilation map [*Zitellini et al*., 2009] and General Bathymetric Chart of the Oceans (GEBCO) digital atlas (http://www.gebco.net/). Thick gray lines labeled P1 and P2 correspond to the WAS profiles acquired during the NEAREST-SEIS survey [*Sallarès et al*., 2011, 2013]. Yellow circles display OBS along the SE segment of the profile P1 presented in this paper (OBS18 to OBS30). Thin gray and green lines correspond to WAS and MCS profiles previously acquired in the area, from N to S: A-AR and B-BR [*Purdy*, 1975], IAM3 [*González et al*., 1996], SW12 and SW13 [*Martínez-Loriente et al*., 2013], SIS-P16 [*Gutscher et al*., 2002], SIS-P4 [*Contrucci et al*., 2004], SIS-P5, SIS-P8, and SIS-P10 [*Jaffal et al*., 2009]. Red stars indicate the location of DSDP sites 120 [*Ryan et al*., 1973] and 135 [*Hayes et al*., 1972]. The estimated continent-ocean boundary (COB) defined in *Sallarès et al*. [2013] is marked as a dashed white line. White circles show epicentral locations of earthquakes with $M_w \geq 3.5$ for the period 1915–2009 (Instituto Geográfico Nacional (IGN) catalog). The focal mechanism solution corresponds to the $M_w = 7.9$, 28 February 1969 event [*Fukao*, 1973]. Purple band displays magnetic anomaly S1 [e.g., *Schettino and Turco*, 2009]. Tectonic structures: solid black lines indicate location of the SWIM strike-slip faults; solid black lines with triangles represent reverse faults, and solid black lines with ticks indicate normal faults (tectonic interpretation after, e.g., *Zitellini et al*. [2009]; *Bartolome et al*. [2012]; *Martínez-Loriente et al*. [2013]). Inset: Global map including the major tectonic plates and boundaries. AGFZ: Azores-Gibraltar Fault Zone; AP: Abyssal plain; CPR: Coral Patch Ridge; CPS: Coral Patch Seamount; GB: Gorringe Bank; GCIW: Gulf of Cadiz imbricated wedge; GF: Gloria Fault; GuB: Guadalquivir Bank; HF: Horseshoe Fault; MPF: Marquês de Pombal Fault; LN: Lineament North; LS: Lineament South; PB: Portimão Bank; PF: Portimão Fault; PSF: Pereira de Sousa Fault; SH: Seine Hills; SVF: São Vicente Fault.

expeditions [e.g., *Auzende et al*., 1984; *Girardeau et al*., 1998], geophysical surveys with seismic and bathymetric data acquisition [e.g., *Purdy*, 1975; *Sartori et al*., 1994; *Banda et al*., 1995; *González et al*., 1996; *Torelli et al*., 1997; *Gutscher et al*., 2002; *Gràcia et al*., 2003a, 2003b, 2010; *Zitellini et al*., 2004, 2009; *Terrinha et al*., 2009; *Sallarès et al*., 2011, 2013; *Martínez-Loriente et al*., 2013], and potential field data modeling [e.g., *Gràcia et al*., 2003b; *Fullea et al*., 2010]. With the aim to investigate the deep structure of the SW Iberian margin, two refraction and wide-angle reflection seismic (WAS) profiles were acquired in 2008 during the NEAREST-SEIS cruise (P1 and P2 in Figure 1) as part of the FP6-EU-funded NEAREST project. Here we present the WAS and gravity modeling results along the SE half of profile P1, which runs from the center of the Horseshoe Abyssal Plain to the Seine Abyssal Plain, crossing the Coral Patch Ridge and the Seine Hills. This section of profile P1 connects the area that is thought to be floored by exhumed serpentinized mantle in the northern part of the Horseshoe Abyssal Plain [*Sallarès et al*., 2013] with the thinned oceanic crust that has been identified south of the Seine Hills [*Contrucci et al*., 2004; *Jaffal et al*., 2009].

The overall objective of this work is to determine the structure and properties of the basement in the Coral Patch Ridge and Seine Hills in order to determine which is the affinity and possible origin of this geological domain. This information, which complements that obtained from WAS modeling along the rest of NEAREST-SEIS profiles [*Sallarès et al*., 2011, 2013], is key to properly understand the regional geodynamic evolution of the area from the Mesozoic to the present day. We first present the data used and methods followed to obtain the velocity and density models along the Coral Patch Ridge to Seine Hills transect. Then, we describe the models and we interpret their lithospheric affinity and geodynamic evolution based on a comparison with previous models. This information is integrated into two regional tectonic and stratigraphic cross sections on the basis of NEAREST-SEIS profiles and synthesized in a map showing the different geological domains. Finally, we suggest a new framework for the geodynamic evolution of the area from the Pangaea breakup to the present-day tectonic plates' configuration that integrates all the models and observations.

2. Geological Setting of the SW Iberian Margin

The SW Iberian margin has undergone a long and complex geodynamic history. Its origin and evolution is framed in a complex setting starting in the Mesozoic with the simultaneous opening of the Western Tethys and the Central Atlantic Oceans in the Lower Jurassic that was followed by the opening of the North Atlantic in the Lower Cretaceous [e.g., *Tucholke et al*., 2007; *Schettino and Turco*, 2009]. The subsequent evolution was controlled by changes in location, geometry, and kinematics of the Eurasian-African plate boundary zone [e.g., *Srivastava et al*., 1990]. After the Lower Oligocene plate reorganization at chron C13n (33.1 Ma), convergent motion between Africa and Eurasia shifted from North Iberia (i.e., along the Pyrenees) to the South, and it was accommodated along its southern margin. Since then, Iberia has been considered as fixed to Eurasia, and so the current plate boundary between North Africa and Iberia was established [*Schettino and Turco*, 2009].

The nature of the basement in this area has been a matter of debate since the first WAS data were acquired in the Tagus and Horseshoe Abyssal Plains in the mid-1970s [*Purdy*, 1975]. Those data were interpreted as corresponding to oceanic crust in the external part of the Gulf of Cadiz, whereas the land recording of the deep multichannel seismic (MCS) IAM3 profile were used to propose the presence of thinned continental crust [*González et al*., 1996] (Figure 1). Other works also dealt with the investigation of the nature of the basement on the basis of potential field data [*Gràcia et al*., 2003b; *Rovere et al*., 2004], generally interpreted as thinned continental crust. More recently, there have been two WAS experiments with ocean bottom seismometers (OBS). The first was the SISMAR cruise, which explored the southern part of the Gulf of Cadiz imbricated wedge (GCIW) (profile SIS-P16) [*Gutscher et al*., 2002], the Moroccan Margin and northern Seine Abyssal Plain (profiles SIS-P4, SIS-P5, SIS-P8, and SIS-P10), suggesting the presence of oceanic crust with variable crustal thickness [*Contrucci et al*., 2004; *Jaffal et al*., 2009] (Figure 1). The second was the NEAREST-SEIS cruise where the two profiles referred above provided strong evidence for the presence of oceanic crust of Jurassic age in the central Gulf of Cadiz (profile P2) [*Sallarès et al*., 2011] and of serpentinized mantle of Early Cretaceous age in the Gorringe Bank and under the sedimentary sequence infilling the southern Tagus and northern Horseshoe Abyssal Plains (NW half of profile P1) [*Sallarès et al*., 2013] (Figure 1).

At the present day, the SW Iberian margin is subjected to a NW-SE compressive regime resulting in active deformation involving old (i.e., Mesozoic) lithosphere [e.g., *Sartori et al*., 1994; *Gràcia et al*., 2003a, 2003b; *Zitellini et al*., 2004; *Terrinha et al*., 2009; *Bartolome et al*., 2012; *Rosas et al*., 2012; *Martínez-Loriente et al*., 2013]. Tectonic activity has shaped a rough seabed morphology characterized by deep abyssal plains separated by NE-SW-oriented prominent highs. In this region, two main types of active faults have been recognized: (a) NE-SW trending thrusts, such as the Marquês de Pombal, São Vicente, Horseshoe, North and South Coral Patch Ridge, and Seine Hills faults [e.g., *Gràcia et al*., 2003a; *Zitellini et al*., 2004; *Terrinha et al*., 2009; *Martínez-Loriente et al*., 2013] and (b) large WNW-ESE trending dextral strike-slip faults (i.e., the SWIM faults), such as the so-called Lineaments North and South faults (LN and LS, respectively) [e.g., *Rosas et al*., 2009; *Terrinha et al*., 2009; *Zitellini et al*., 2009; *Bartolome et al*., 2012; *Martínez-Loriente et al*., 2013] (Figure 1).

The seismicity recorded in the study area mostly concentrates north of the LS, between the Gorringe and Portimão banks [*Zitellini et al*., 2009] (Figure 1). A local network of OBS deployed in the area in 2007 recorded numerous low- to moderate-magnitude earthquakes of $M_L = 2.2–4.8$ that concentrate at a depth of 40–60 km, with only few events nucleating shallower than 20 km [*Geissler et al*., 2010]. Moment tensor inversions of these earthquakes reveal WNW-ESE-trending nodal planes with a reverse and right-lateral slip [*Geissler et al*.,

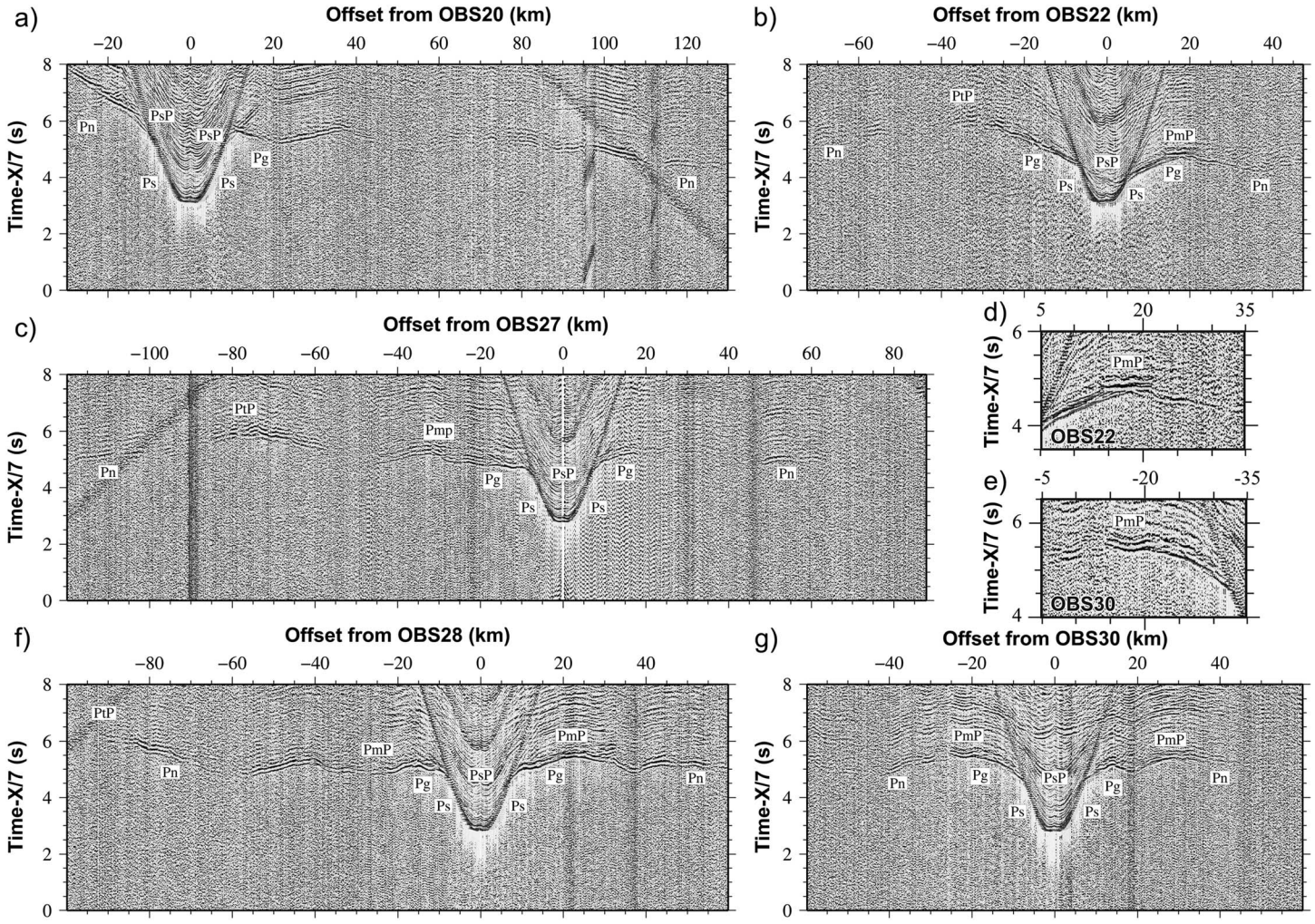

Figure 2. Recorded seismic sections corresponding to the vertical component of (a) OBS20, (b) OBS22, (c) OBS27, (f) OBS28, (g) OBS30, and blow up of the (d) OBS 22 and (e) 30 showing PmP phase in detail, deployed along P1 (Figure 1). The vertical axis represents reduced traveltime (in seconds), and the horizontal axis is offset from OBS position (in km). Band-pass (5–15 Hz) and automatic gain control (AGC) filtering was applied to the raw data. Reduction velocity is 7 km/s. The white labels indicate the seismic phases that have been identified and modeled (see text for description).

2010]. The nucleation of earthquakes at these depths, combined with the structure and nature of the basement in different parts off SW Iberia based on combined WAS and gravity models [*Sallarès et al*., 2011, 2013], suggests that they occur within the upper mantle [e.g., *Stich et al*., 2010; *Bartolome et al*., 2012]. Therefore, combining geological and geophysical information to infer the nature of the basement in each domain is a key aspect that needs to be taken properly into account to evaluate the regional seismic and tsunami hazard.

3. Modeling Results

3.1. Data Acquisition

The 340 km long NEAREST profile P1 was acquired during fall 2008 onboard the Spanish R/V *Hesperides*. Twenty-nine OBS were deployed along the profile from the Tagus Abyssal Plain at the northwest to the Seine Abyssal Plain at the southeast, crossing the Gorringe Bank, the Horseshoe Abyssal Plain, the Coral Patch Ridge, and the Seine Hills. The NW part of this profile, from the Tagus Abyssal Plain to the central part of the Horseshoe Abyssal Plain, was modeled and interpreted by *Sallarès et al*. [2013]. In this work we present the whole velocity model including the unpublished SE half of the profile, which is 160 km long and includes recordings at 13 OBS apart from the 18 OBS that were already modeled in the NW part of this profile, 6 of the short-period L-Cheapo 4 × 4 model from the Spanish UTM-CSIC pool, and 7 of the MicroOBS model from the French IFREMER-IUEM pool [*Auffret et al*., 2004]. The seismic source used in the experiment was composed of two arrays with seven Bolt air

guns (model 1500 LL), providing a total volume of 0,071 m^3. The arrays were deployed at a depth of 12 m, and the shot interval was set to 90 s (~210 m) to avoid noise generated by previous shots.

The OBS recorded data have a good quality overall (Figure 2 and supporting information), especially the first arrivals. The water wave arrival was used to relocate the instruments in the seafloor using a grid search algorithm, and clock-drift corrections were also calculated. The data preprocessing is the same that was applied to the rest of record sections along the two profiles and included a de-bias, a whitening deconvolution, a butterworth band-pass filter (4–18 Hz), and an AGC filtering.

3.2. Phase Picking and Joint Refraction and Reflection Traveltime Inversion Method

A total of 20,022 picks were manually picked in the 30 OBS deployed along profile P1 (16,130 of which correspond to the unpublished 13 OBS located in this SE half of the profile), including sedimentary (Ps), intracrustal (Pg), and upper mantle (Pn) refracted phases; and reflections at the sediment-basement interface (PsP), at the crust-mantle (PmP) boundary in the Seine Abyssal Plain, and at a deeper structure located in the middle of the Horseshoe Abyssal Plain (PtP) (Figure 2). PmPs interpreted to be reflections at the Moho boundary were identified in this SE half of the profile that includes the Coral Patch Ridge and Seine Abyssal Plain areas, whereas they are lacking in the NW half that encompasses the Tagus and Horseshoe Abyssal Plains and the Gorringe Bank [*Sallarès et al*., 2013]. A picking uncertainty of the order of half of the dominant signal period (~10 Hz) was assigned to the traveltime picks accounting for potential picking errors and a possible systematic shift. For Ps, Pg, and near-offset Pn phases, the average uncertainty was ~50 ms, while it was ~70 ms for far-offset Pn's, PsP's, PmP's, and PtP's.

The 2-D velocity model was obtained using the *tomo2d* joint refraction and reflection traveltime inversion code [*Korenaga et al*., 2000]. This method allows the determination of the velocity model and the geometry of a floating reflector from the simultaneous inversion of traveltimes from first arrivals and from a single reflected phase at a time. Traveltimes and ray paths are calculated using a hybrid ray-tracing scheme based on the graph method with a local ray bending refinement [*Moser et al*., 1992]. The iterative linearized inversion is regularized applying smoothing constrains for predefined correlation lengths and damping factors (weighting parameters to stabilize the linear system of the inversion; i.e., a higher value of damping means less modification in the inversion) for the model parameters [*Korenaga et al*., 2000]. The derivative weight sum (DWS) is the column-sum vector of the velocity kernel [*Toomey and Foulger*, 1989] and measures the ray coverage, providing information on the linear sensitivity of the inversion. Our grid spacing is $\Delta x = 500$ m and $\Delta z = 50$ m immediately below the seafloor to 500 m in the bottom of the model, and the smoothing correlation lengths are 2–8 km, from top to bottom, horizontally, and 0.25–2.0 km, from top to bottom, vertically.

A three-step layer-stripping procedure was followed consisting of adding the data sequentially, starting from the shortest offsets/uppermost levels and finishing with the longest offsets/deepest levels as described in *Sallarès et al*. [2011]. This strategy allows accounting for sharp velocity contrast across geological interfaces such as the sediment-basement or the crust-mantle boundary. In the first step we inverted traveltimes from the sediment phases alone (Ps and PsP) to determine the velocity field of the sedimentary layer and the geometry of the sediment-basement interface. The damping parameter for velocity and depth in the first inversion is 15% (i.e., the maximum change allowed for all model parameters between successive iterations is 15% of the absolute value). In the second step we incorporated also the basement phases, which in the SE half of the profile include the Pg and PmP arrivals, apart from the Ps, to obtain the crustal velocity distribution and Moho geometry. In this step we included the inverted velocity model of the sediments as initial model, with a damping factor of 100 to 1 for the parameters of the sedimentary layers, to let it modify the model preferably the crust. The starting velocity model below the sediment boundary was a 1-D model starting at 5 km/s and with a constant velocity gradient of 0.33 s^{-1}. The initial Moho reflector was set at 6 km below the sediment-basement boundary. In the last step we incorporated the Pn and PtP phases to obtain the upper mantle velocity distribution and the geometry of the deep floating reflector located beneath the Horseshoe Abyssal Plain. In this last step the previously obtained model that comprises sediments and crust was included as initial model, with a damping factor of 100 to 1 for the parameters of the crust and sedimentary layers, to let it modify preferably the upper mantle. The starting velocity model below the Moho in the SE half was a 1-D model starting at 7.8 km/s and with a constant velocity gradient of 0.02 s^{-1}.

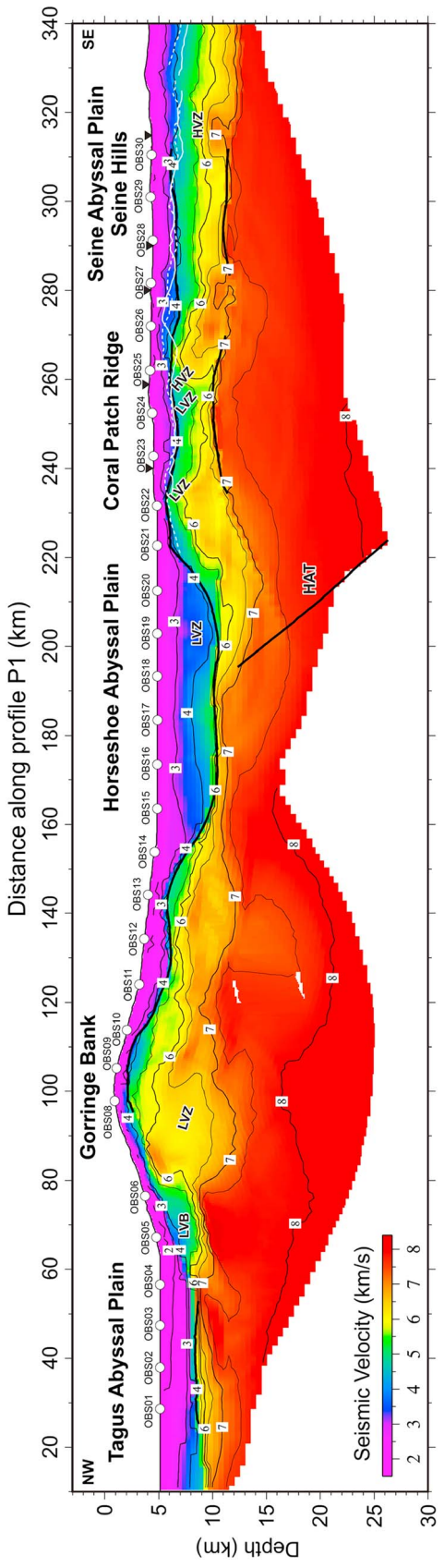

Figure 3. The 2-D final velocity model obtained by joint refraction and reflection traveltime inversion of the whole data set, composed of arrival times of Ps, PsP, Pg, PmP, Pn, and PtP phases (see text for definitions). The first half of the profile (0–190 km) is published by *Sallarès et al.* [2013]. Thick solid black lines display the inverted sediment-basement boundary, the crust-mantle boundary (i.e., Moho), and the Horseshoe Abyssal plain Thrust (HAT). The dashed and solid white lines correspond to the horizons interpreted to be the base of the sediment cover along the MCS profiles SW12 and SW13, respectively [*Martínez-Loriente et al.*, 2013] (see location in Figure 1). White circles indicate OBS locations. Inverted black triangles indicate the location of the 1-D *P* wave velocity/depth profiles shown in Figure 6. Velocity units are km/s. HVZ: high-velocity zone; LVZ: low-velocity zone; LVB: low-velocity body.

The final 2-D velocity model is presented in Figure 3, whereas several representative examples of record sections with the interpreted phases are shown in Figure 2 (the corresponding picks, traveltime fits, and ray paths are presented as supporting information). These record sections complement those recorded in the NW part of the profile, which are shown in *Sallarès et al.* [2013]. The final root-mean-square (RMS) residual of the model is 61 ms, giving a chi-square value of 0.89. The DWS of the final velocity model is shown in Figure 4a.

3.2.1. Uncertainty of the Velocity Model Parameters

In order to estimate the uncertainty of our model parameters (Figure 3) due to a combination of the starting model selected, the experiment geometry, the theoretical approximation made, and data picking errors, we performed a Monte Carlo-type stochastic error analysis. The approach followed [*Korenaga et al.*, 2000; *Sallarès and Ranero*, 2005; *Sallarès et al.*, 2005] consist of randomly perturbing the reference velocity model and the reflector depth within reasonable bounds according to a priori lithological information, generating a set of 300 2-D starting models and reflectors. In our case, velocity nodes have been perturbed by ±0.7 km/s and the Moho reflector has been varied ±0.5 km. Together with the perturbed velocity models, we used 300 noisy data sets generated by adding random common phase errors (±20 ms), common receiver errors (±20 ms), and individual picking errors (±20 ms) to the initial data set. Then the inversion is repeated for 300 randomly selected perturbed velocity models-noisy data set pairs, using the inversion parameters described in the previous section. The mean deviation of all inversions can be interpreted as a statistical measure of the model parameters uncertainty [*Tarantola*, 1987]. The mean deviation of the 300 inverted final models and the error bars of all interfaces are shown in Figure 4b, whereas the result from 0 to 200 km along the profile was first presented in *Sallares et al.* [2013].

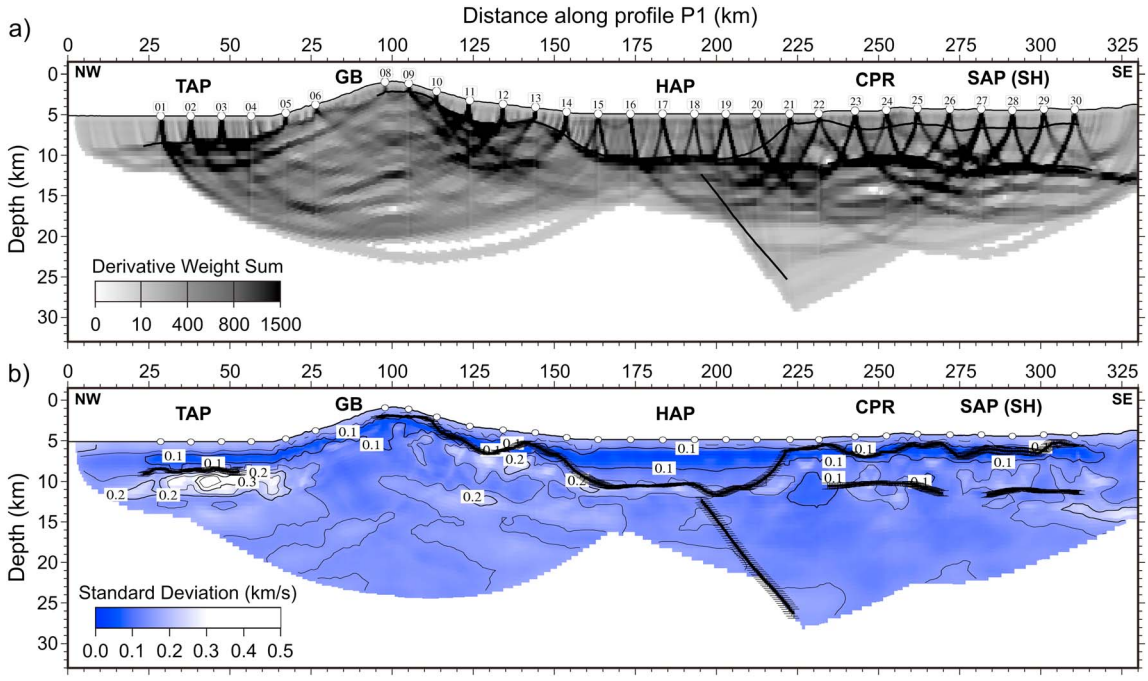

Figure 4. (a) Derivative weight sum for the 2-D velocity model shown in Figure 3. (b) Velocity uncertainty for the 2-D model shown in Figure 3. It corresponds to the mean deviation of the 300 solutions obtained in the stochastic Monte Carlo analysis (see text for details). Velocity units are km/s. White circles indicate OBS locations. GB: Gorringe Bank; CPR: Coral Patch Ridge; HAP: Horseshoe Abyssal Plain; SAP: Seine Abyssal Plain; SH: Seine Hills; TAP: Tagus Abyssal Plain.

3.3. Gravity Modeling

The final velocity model (Figure 3) has been complemented with gravity modeling. The gravity analysis was done converting the WAS-derived seismic velocity to density using different empirical velocity-density relationships for each geological layer assuming a given lithological composition, similar to what is done in *Sallarès et al*. [2000]. In the case of the sedimentary cover, we used *Hamilton*'s [1978] law for shale. In the case of the basement, we tested three different empirical relationships according to the three possible interpretations for the nature of the layer below the sedimentary cover (i.e., continental crust, exhumed serpentinized mantle, or oceanic crust). For continental crust we used *Christensen and Mooney*'s [1995] relationship, for the exhumed mantle we used *Carlson and Miller*'s [2003] relation for low-T serpentinized peridotite, and for oceanic crust we employed *Carlson and Herrick*'s [1990] which is valid for layer 2/3 basalts and gabbros. These are the same relationships that were previously tested in the NW part of profile P1 [*Sallarès et al*., 2013]. Density and velocity were corrected from in situ to laboratory conditions and vice versa using experimental estimates of pressure (*P*) and temperature (*T*) partial derivatives for oceanic and continental crust [*Korenaga et al*., 2001] and for serpentinized peridotite [*Kern and Tubia*, 1993]. The aim is to check if the density model obtained is compatible with the observed free-air gravity data [*Sandwell and Smith*, 2009]. To calculate the gravity anomaly generated by a vertically and laterally heterogeneous 2-D density model, we used a code based on *Parker*'s [1974] spectral method as implemented by *Korenaga et al*. [2001].

4. Results

4.1. Description of the Velocity Model From the Coral Patch Ridge to the Seine Abyssal Plain

In this section the final velocity model of the SE part of the NEAREST profile P1 (from 180 to 340 km) is described, whereas the NW part is presented in *Sallarès et al*. [2013] (Figure 3).

The thickness of the sedimentary cover obtained after the first inversion step using Ps and PsP phases differs considerably between the Horseshoe and the Seine Abyssal Plains. In the Horseshoe Abyssal Plain it reaches a maximum thickness of ~5 km, whereas in the Coral Patch Ridge and Seine Hills areas it varies between a

minimum of 1 km in the top of a basement high and a maximum of 2.5 km in a local basin (Figure 3). In this region the sedimentary cover is known to be composed of Mesozoic and Cenozoic sediments [*Hayes et al*., 1972] and has been largely studied and characterized in detail using (MCS) data [e.g., *Sartori et al*., 1994; *Tortella et al*., 1997; *Hayward et al*., 1999; *Zitellini et al*., 2009; *Martínez-Loriente et al*., 2013]. There is a good correspondence between the WAS-derived sediment-crust boundary and the base of the sediment cover in the MCS profiles SW12 and SW13 from *Martínez-Loriente et al*. [2013] that intersect the SE half of the profile P1 (Figures 1 and 3). The correspondence is poorer between OBS 25 and 27 probably because the depth of the sediment-crust boundary is less controlled, as shown by the corresponding uncertainty bars (Figure 4b). The sedimentary units show velocities ranging from ~1.8 km/s just below the seafloor to 4.0 km/s at the base of the sediment-basement boundary, although they locally reach up to ~5.0 km/s in the deeper part of the Horseshoe Abyssal Plain, corresponding to consolidated Mesozoic sediments [e.g., *Martínez-Loriente et al*., 2013] (Figure 3). Below OBS 19 (~203 km along profile) the contours of the velocity field reflect a negative anomaly in the sedimentary layer that might continue below the sediment-basement boundary.

The crust underlying the sedimentary cover in the SE half of the profile is thin and laterally heterogeneous (Figure 3). From 200 to 305 km the thickness ranges from 3.5 to 5.5 km, while in the southernmost part (305 to 340 km) it is slightly thicker, reaching 5.5–6.0 km. Crustal velocities vary from 4.0–5.0 km/s at the top to 7.0–7.1 km/s at the crust-mantle boundary, with a vertical velocity gradient twice stronger in the uppermost crust than in the lower crust (Figure 3). The presumed Moho reflector is locally disrupted as observed between 270 and 285 km in Figure 3, because PmP phases have not been identified in all the corresponding record sections, only in nine of the OBS. A striking feature of the tomographic model is the highly heterogeneous velocity distribution in the Seine Abyssal Plain, showing low- and high-velocity anomalies that are especially marked between 230 and 285 km. The irregular character of the velocity contours in the sedimentary layer above these anomalies, and especially from ~3 km deep down to the Moho, indicate that these features probably affect the whole crust. Between 285 and 340 km the velocity field is more uniform, except for a small NW dipping high-velocity anomaly centered at 315–320 km that affects the lower part of the crust.

In the center of the Horseshoe Abyssal Plain (190–200 km) there is an abrupt lateral change in the basement velocity field. In this place the velocity just below the sediment-basement boundary abruptly changes from "normal" upper crustal velocities of ~5 km/s to the south to velocities as high as ~7.0 km/s to the north, which corresponds to the part of the profile presented by *Sallarès et al*. [2013]. The upper mantle is sampled by Pn phases up to ≤ 12 km below the Moho between 200 and 280 km, diminishing to the SE end of the profile. The mantle velocity reaches values as low as ≤7.5 km/s in the shallowest upper mantle, quite low as compared with typical upper mantle velocities of 8.0–8.3 km/s [*Carlson and Miller*, 2003].

Uncertainty in the SE part of the profile within the sedimentary layer is low (≤0.1 km/s), increasing to ~0.15 km/s near the top of the basement between 180 and 200 km, where a sharp velocity contrast between the sediments and the basement occurs (Figure 4). Velocity uncertainty within the basement is also low (≤0.1 km/s), including the region where the low- and high-velocity anomalies have been identified (from 230 to 285 km) (Figure 4). Velocity uncertainty in the uppermost mantle is also ≤0.15 km/s, except in the southernmost part of the profile where it increases to ~0.2 km/s due to the poor ray coverage at the end of the profile (Figure 4). The generally low velocity uncertainties, which are uncertainties in mean velocity over the correlation lengths used in the inversion, confirm that the velocity field obtained is remarkably well constrained by the data (Figures 3 and 4). The sediment-basement boundary in this part of the profile has an average uncertainty of ±0.3 km that increases to ±0.8 km from ~270 km. The interpreted Moho has an average uncertainty of ±0.5 km, while the average uncertainty of the Horseshoe Abyssal plain Thrust (HAT) geometry is ±0.7 km (Figure 4).

4.2. Velocity-Derived Density Structure

The comparison between the satellite-derived free-air gravity anomaly [*Sandwell and Smith*, 2009] and the calculated gravity anomaly for each of the density models generated using the velocity-density relationships for the different lithologies allows discerning between the different hypotheses. However, it must be noted that the long-wavelength anomalies can be affected by factors other than the compositional one, so that the interpretation based on the gravity data alone must be carefully taken. The gravity model of the NW part of the profile was presented by *Sallarès et al*. [2013]. Making a similar analysis, the authors concluded that the best fit with the satellite-derived free-air anomaly data was obtained by transforming the basement velocity model into density using *Carlson and Miller*'s [2003] relation for serpentinized peridotite.

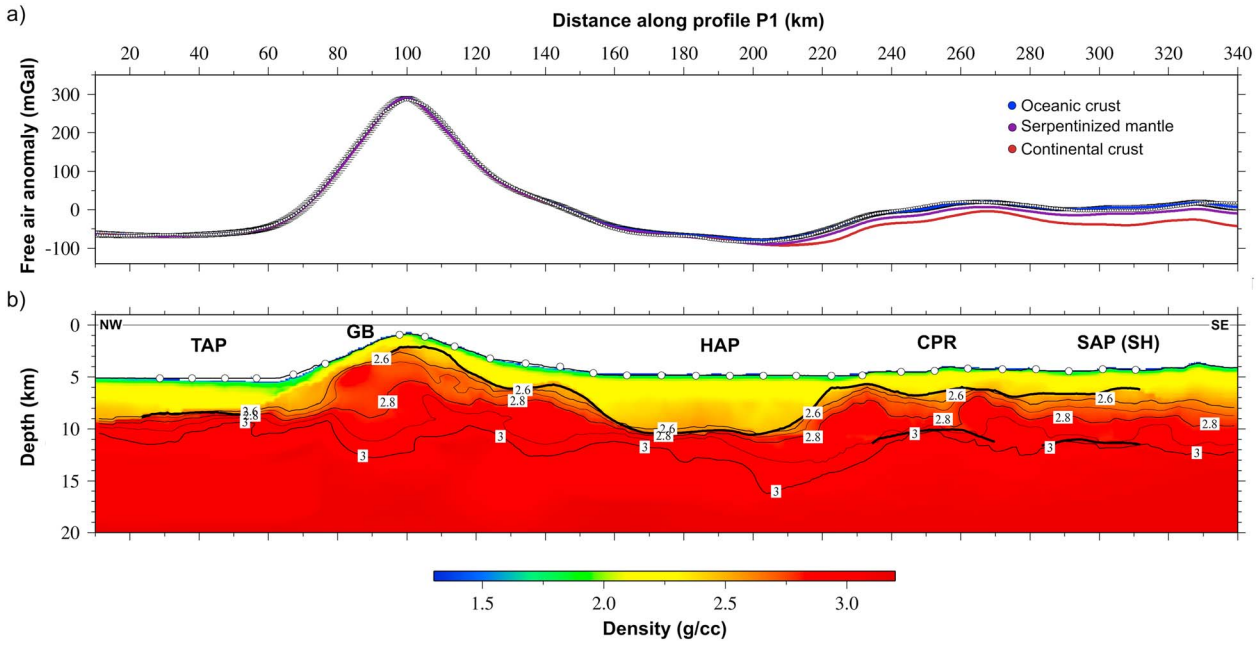

Figure 5. (a) Observed free-air gravity anomaly (dotted line) and calculated gravity anomalies for the velocity-derived density model using different empirical relationships for the layer beneath the sedimentary cover in the southern half of profile P1: the oceanic crust model displayed in Figure 5b (blue line, RMS = 5.1 mGal) using *Carlson and Herrick*'s [1990] relationship; the *Carlson and Miller*'s [2003] relationship for serpentinized mantle (purple line, RMS = 7.2 mGal); and the *Christensen and Mooney*'s [1995] relationship for continental crust model (brown line, RMS = 15.6 mGal). Error bars indicate gravity anomaly uncertainty inferred from the Monte Carlo analysis (Figure 4b). (b) Velocity-derived density model along P1 transforming the velocity model in Figure 3, to density (ρ) using *Hamilton*'s [1978] law for shale in the sediments ($\rho = 0.917 + 0.747V_p - 0.08V_p^2$), *Carlson and Miller*'s [2003] relationship for serpentinite ($\rho = 1.577 + 0.196V_p$) in the basement between 0 and 190 km and beneath the crust layer between 190 and 340 km, and *Carlson and Herrick*'s [1990] relationship for oceanic crust ($\rho = 3.81 - 6.0/V_p$) in the crust layer between 190 and 340 km. Density units are g/cm^3. White circles indicate OBS locations. GB: Gorringe Bank; CPR: Coral Patch Ridge; HAP: Horseshoe Abyssal Plain; SAP: Seine Abyssal Plain; SH: Seine Hills; TAP: Tagus Abyssal Plain.

We have integrated both the NW and SE parts of the profile to construct a single model of the whole transection. In the NW half we have inserted *Sallarès et al.*'s [2013] model, which was built using *Hamilton*'s [1978] law for sediments, and *Carlson and Miller*'s [2003] relation for low-T serpentinized peridotite for the basement. In the SE part we tested three different relationships based on the three possible interpretations for the nature of the basement according to the regional geology and previous work (i.e., continental crust, exhumed serpentinized mantle, and oceanic crust). In the upper mantle we have used *Carlson and Miller*'s [2003] relation for serpentinite in the three cases.

Figure 5a shows the comparison between the calculated gravity anomaly for the three resulting density models together with the observed gravity anomaly. The model obtained using *Carlson and Herrick*'s [1990] conversion for oceanic crust provides the best fit with the observed anomaly, with a root-mean-square (RMS) misfit of 5.1 mGal. In the case of *Carlson and Miller*'s [2003] relation for low-T serpentinized peridotite, the fit obtained is reasonably good with an RMS slightly higher than in the previous case (7.2 mGal). The gravity response of the density model obtained using *Christensen and Mooney*'s [1995] relation for continental crust is the worst, with an RMS of 15.6 mGal.

5. Discussion

The discussion of the velocity and density models presented in Figures 3 and 5 is structured in four parts. First, we compare our modeling results with previous interpretations regarding the nature of the basement rocks in the SE half of the profile and we make an interpretation of the basement affinity based on this comparison. Then, we discuss the nature of the transition between this area and the NW part of the profile presented in *Sallarès et al*. [2013]. Next, we propose a plausible present-day configuration of crustal domains off the SW Iberian margin based on the geological interpretation of all the WAS data acquired during the NEAREST-SEIS survey (profiles P1 and P2 in Figure 1) (i.e., this work and *Sallarès et al*. [2011, 2013]) together with other data and information available from the region. We finally propose a plausible framework for the geodynamic

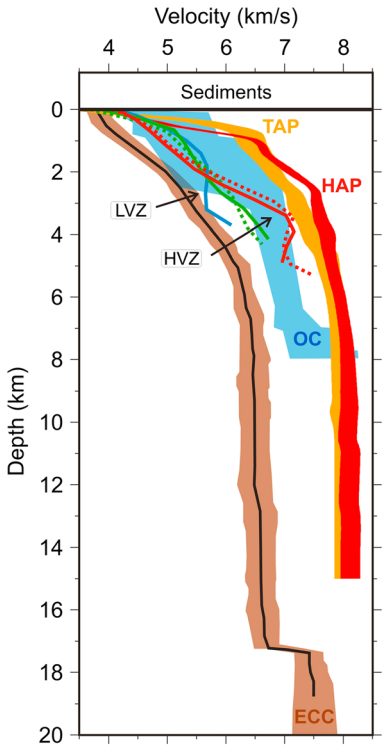

Figure 6. The 1-D *P* wave velocity/depth profiles representative of the various segments along the thin crust of profile P1: thin oceanic crust (240 km and 290 km, green lines), across high-velocity anomalies (280 km and 317 km, red lines), across low-velocity anomaly (258 km, blue line), compared with previous results for >140 Ma Atlantic oceanic crust [*White et al.*, 1992, Figure 6] (blue area); exhumed mantle at the Horseshoe Abyssal Plain (170–180 km along profile P1; red band) and at the Tagus Abyssal Plain (35–45 km along profile P1; orange band) [*Sallarès et al.*, 2013]; and extended continental crust at the SW Iberian margin from NEAREST-SEIS profile P2 (190 km along profile P2; brawn band) [*Sallarès et al.*, 2011]. The width of the band in the velocity profiles correspond to the uncertainty bounds. ECC: extended continental crust; HAP: Horseshoe Abyssal Plain; HVZ: high-velocity zone; LVZ: low-velocity zone; OC: Oceanic Crust; TAP: Tagus Abyssal Plain.

evolution of the SW Iberian margin since the early phases of the Central Atlantic opening to the present day, integrating all the observations.

5.1. Interpretation of the Velocity and Velocity-Derived Density Models

The final velocity model (Figure 3) displays a 1.0–2.5 km thick sedimentary layer in the Coral Patch Ridge and Seine Abyssal Plain areas that overlays the basement. Concerning the nature of the basement, there are three possible interpretations: continental crust, exhumed mantle, or oceanic crust. The Deep Sea Drilling Project (DSDP) Site 135 located on top of the Coral Patch Ridge (~260 km along profile) did not reach the basement [*Hayes et al.*, 1972]. In the absence of direct basement samples or well-defined magnetic anomalies, the best available indicator of the nature of the crust is the velocity structure and crustal thickness obtained from combined WAS and gravity data modeling.

The differences between the velocity structure of the Seine Abyssal Plain with that corresponding to extended continental crust of the SW Iberian margin, obtained along the NEAREST-SEIS profile P2 [*Sallarès et al.*, 2011] (Figure 6), are clear concerning both absolute velocity and vertical velocity gradients. Furthermore, as indicated in the previous section, the velocity-derived density model obtained using a continental crust relationship [*Christensen and Mooney*, 1995] does not fit with the observed gravity anomaly along the whole SE part of the profile (Figure 5). The velocity model fits significantly better with a reference for the exhumed mantle rock basement described in Horseshoe and Tagus Abyssal Plains [*Sallarès et al.*, 2013] (Figure 6). However, the basement velocities of our model are generally slower, and the velocity gradients are slightly lower in comparison with these reference models (Figure 6). The velocity-derived density model obtained using *Carlson and Miller*'s [2003] relation for serpentinized peridotite explains reasonably well the observed gravity anomaly (Figure 5). Therefore, the combined WAS and gravity modeling do not allow to rule out the hypothesis of an exhumed mantle rock affinity for the basement in the Coral Patch Ridge and Seine Abyssal Plain areas, as it has been previously proposed for the Horseshoe and Tagus Abyssal Plains. However, an observation that is difficult to reconcile with this hypothesis is the identification of wide-angle reflections consistent with the presence of a well-developed crust-mantle boundary (PmP) in a number of OBS deployed in the Coral Patch Ridge and Seine Abyssal Plain (Figure 2), which is not the case for the OBS deployed in the Horseshoe and Tagus Abyssal Plains and Gorringe Bank.

The last option that has been analyzed is the oceanic crust hypothesis. The thickness of the crust identified in the Coral Patch Ridge and Seine Abyssal Plain areas (3.5–6.0 km thick) is in good agreement with the thin oceanic crust imaged in the SISMAR WAS profile SIS-P5 (4–6 km thick), which was acquired just south of the Seine Hills [*Jaffal et al.*, 2009] (Figure 1). The crust identified in our model displays a 2–3 km thick upper layer with a velocity of 4.0–6.5 km/s that according to its velocity and velocity gradient could well correspond to oceanic layer L2, and a 0.5–3 km thick lower layer with velocities of 6.5–7.0 km/s, which could represent oceanic L3. In fact, the velocity and velocity gradient of these two layers are within the range of velocity corresponding to a normal, Atlantic-type, >140 Ma old oceanic crust [*White et al.*, 1992]. The main difference between our model and a normal oceanic crust is the thickness of layer L3, which is substantially

thinner than the 4–5 km that is commonly observed [e.g., *White et al*., 1992] (Figure 6). This velocity structure with a normal thickness L2 but a thinner-than-normal L3 is comparable to that described in oceanic crust generated at slow- and/or ultraslow-spreading centers. Well-known examples are the WAS profiles acquired in the ultraslow South-West Indian Ridge (SWIR) [*Muller et al*., 2000; *Minshull et al*., 2006] (Figure 6) and at the ultraslow Arctic mid-ocean ridges [*Dick et al*., 2003]. In the studied segment of the SWIR, the half-spreading rate is 6–12 mm/yr [e.g., *Muller et al*., 2000; *Minshull et al*., 2006]. *Minshull et al*. [2006] suggested that the "crustal" material in these areas would consist at least partly of serpentinized mantle rocks. As their *P* wave velocities can be typical of L3 (i.e., 6.5–7.0 km/s) or as low as 4–5 km/s if the rocks are highly serpentinized and strongly altered [e.g., *Miller and Christensen*, 1997], it is difficult to seismically distinguish from basaltic and gabbroic rocks. In addition, the excellent fit of the velocity-derived density model obtained with a conversion law specific for oceanic crust [*Carlson and Herrick*, 1990], which gives the lowest RMS and is the only one that is within the error bars inferred from the Monte Carlo analysis, also supports this argument (Figures 4b and 5). Nevertheless, the velocity structure is highly heterogeneous, with low- and high-velocity anomalies, and the Moho is not continuous but appears to be severely disrupted. The local presence of serpentinized mantle rocks could explain the high-velocity anomalies identified between 270–280 km and 310–320 km along the profile. It is noteworthy that these two segments coincide with the places where PmP reflections have not been identified in the record sections (Figures 2 and 3).

The SE dipping low-velocity anomalies identified in the crust are reflected in the 1-D *P* wave velocity/depth profiles shown in Figure 6. These anomalies may be the tomographic expression of fault-related rock fracturing that could have promoted rock alteration by fluid percolation. The uppermost mantle velocity below the crust shows an average velocity of $\leq$7.5 km/s, 10–12% slower than normal, unaltered pyrolitic mantle (8.1–8.2 km/s) (Figure 3). This low velocity may be indicative of serpentinization at upper mantle levels, which would in turn indicate that the faults identified might cross the Moho and penetrate at least 3–4 km into the upper mantle. Additionally, the location of the low-velocity anomalies coincide reasonably well with the active structures recently described in that area with MCS profiles [*Martínez-Loriente et al*., 2013] (Figure 3).

5.1.1. Transition Between the Serpentinized Peridotite Basement in the NW Horseshoe Abyssal Plain and the Oceanic Crust in the Coral Patch Ridge

As previously mentioned, there is a sharp lateral velocity change at the top of the basement in the center of the Horseshoe Abyssal Plain (190–200 km along profile P1), where the uppermost basement velocity increases by $>$25% (Figure 3) within a distance of ~10 km. According to our interpretation, this velocity change must represent a boundary between two different geological domains: (1) the basement interpreted to be composed of exhumed mantle rocks identified in the northern part of the Horseshoe Abyssal Plain, the Gorringe Bank, and the southernmost Tagus Abyssal Plain described by *Sallarès et al*. [2013] and (2) an oceanic crust such as the one described and discussed in previous sections and also that interpreted in the central Gulf of Cadiz by *Sallarès et al*. [2011]. The presence of a different basement affinity north and south of the Coral Patch Ridge is also consistent with the bathymetric data, showing that the seafloor is ~400 m deeper in the Horseshoe Abyssal Plain than in the Seine Abyssal Plain. If the sedimentary layer of the model is not considered, the difference is even larger, with the top of the basement located 2–3 km deeper in the central Horseshoe Abyssal Plain than in the Seine Hills of the Seine Abyssal Plain [*Martínez-Loriente et al*., 2013]. As indicated by the gravity analysis, these differences are also in agreement with the presence of a denser, less buoyant basement in the Horseshoe Abyssal Plain (i.e., exhumed mantle) than in the Seine Abyssal Plain (i.e., igneous crust).

In this context, a question remains concerning the type of transition between these two domains. An observation that may help to better understand this transition is the presence of faint, deep reflections in the record sections of six OBS located SE of the Coral Patch Ridge (PtP in Figure 7). The inversion of PtP arrival times shows that these reflections should correspond to a deep, SE dipping feature located in the middle of the Horseshoe Abyssal Plain, just beneath the transition area toward the Coral Patch Ridge (Figure 3). According to our models, the dip angle of this structure should be ~30°, although it must be noted that this value may be an apparent dip because there is only one profile crossing it; thus, there is no 3-D information about this structure. This feature, which is interpreted to separate the two above mentioned regions, will be hereafter referred to as the Horseshoe Abyssal plain Thrust (HAT). To estimate the dip uncertainty of the HAT, we randomly perturbed the dip of the initial reflector used in the inversion by $\pm$ 20° so that the initial dip was

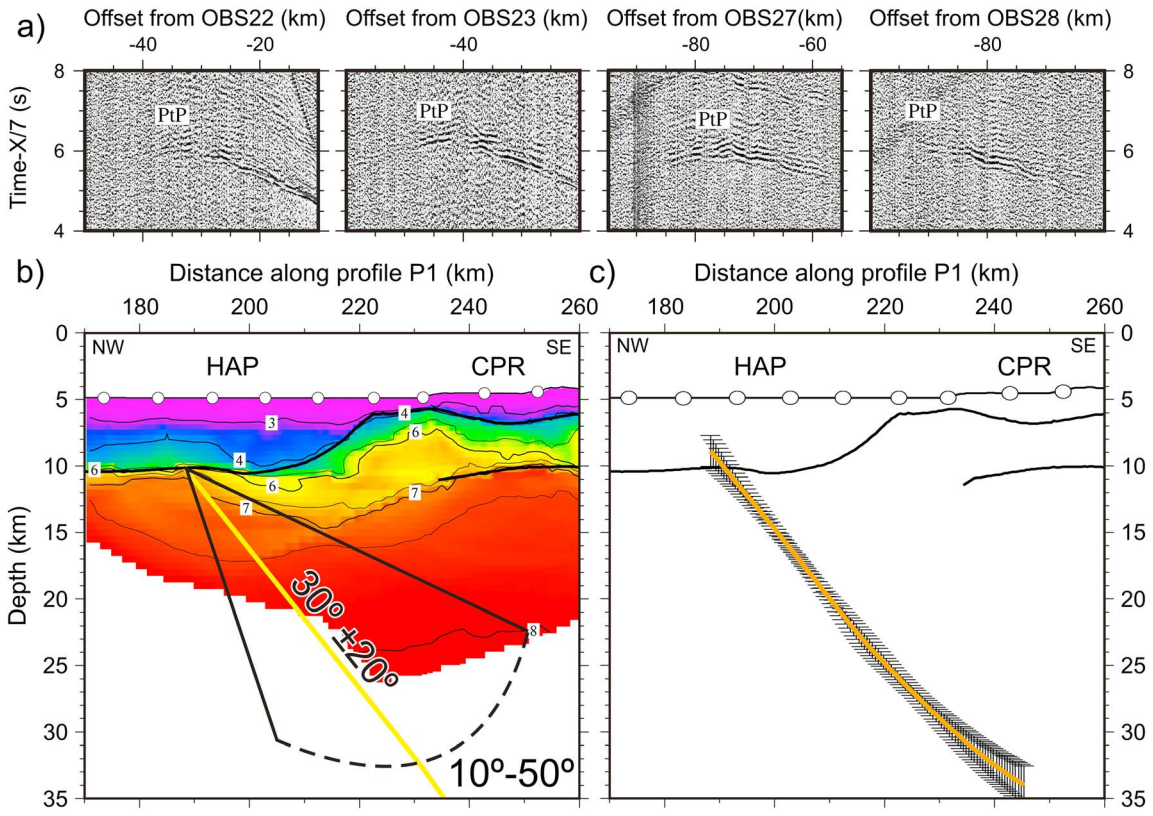

Figure 7. (a) Zoom of the recorded seismic sections corresponding to the vertical component of OBS22, OBS23, OBS27, and OBS28, deployed along P1, illustrating the PtP phase. (b) Sketch of the initial configuration of the 500 reflectors used in the stochastic Monte Carlo analysis performed to analyze the uncertainty of the HAT geometry. (c) Mean of the 500 solutions obtained in the stochastic Monte Carlo analysis with the corresponding error bars (see text for details). Vertical exaggeration = ~2.4. CPR: Coral Patch Ridge; HAP: Horseshoe Abyssal Plain.

10°–50°, whereas the velocity model was that shown in Figure 3. The average geometry of the HAT obtained from all inversions with the corresponding error bars, which correspond to the mean deviation with respect to the average dip, are all shown in Figure 7.

5.2. Geological Domains off the SW Iberian Margin

In this section we combine the interpretation of the WAS profile presented in this paper with the ones presented in previous works [*Sallarès et al.*, 2011, 2013] to construct two new geological cross sections integrating tectonic and stratigraphic information (Figure 8). Then, we combine our WAS results with complementary information provided by previous WAS models [*González et al.*, 1996, 1998; *Gutscher et al.*, 2002; *Contrucci et al.*, 2004; *Jaffal et al.*, 2009; *Palomeras et al.*, 2009], potential field data [e.g., *Gràcia et al.*, 2003b; *Fullea et al.*, 2010], available MCS data [e.g., *Sartori et al.*, 1994; *Banda et al.*, 1995; *Torelli et al.*, 1997; *Tortella et al.*, 1997; *Maldonado et al.*, 1999; *Hayward et al.*, 1999; *Gràcia et al.*, 2003a, 2003b; *Medialdea et al.*, 2004; *Zitellini et al.*, 2004; *Iribarren et al.*, 2007; *Terrinha et al.*, 2009; *Bartolome et al.*, 2012; *Martínez-Loriente et al.*, 2013], and geological information from scientific and commercial wells [e.g., *Hayes et al.*, 1972; *Ryan et al.*, 1973; *Lanaja et al.*, 1987] and seafloor rock dredges [e.g., *Baldy et al.*, 1977; *Malod and Mougenot*, 1979; *Hinz et al.*, 1984] (Figure S2 in supporting information) to construct the first regional map of the basement domains in the SW Iberian margin (Figure 9).

5.2.1. Geological Cross Section Along Profile P1: From the Tagus Abyssal Plain to the Seine Hills

The basement of the NW half of the profile, which runs from the Tagus Abyssal Plain to the center of the Horseshoe Abyssal Plain, is likely to be made of partially serpentinized, exhumed mantle peridotites [*Sallarès et al.*, 2013] (Figures 8a and 9), which were originally part of a wide band of exhumed mantle rocks similar to the zone of exhumed continental mantle (ZECM) of the Iberia Abyssal Plain [*Pinheiro et al.*, 1992; *Dean et al.*, 2000; *Srivastava et al.*, 2000; *Whitmarsh et al.*, 2001]. This band was generated by tectonic mantle denudation at the beginning of the North Atlantic opening (147–133 Ma); therefore, it may well constitute the southernmost and oldest section of the West Iberian margin continent-ocean transition (COT) [*Schettino*

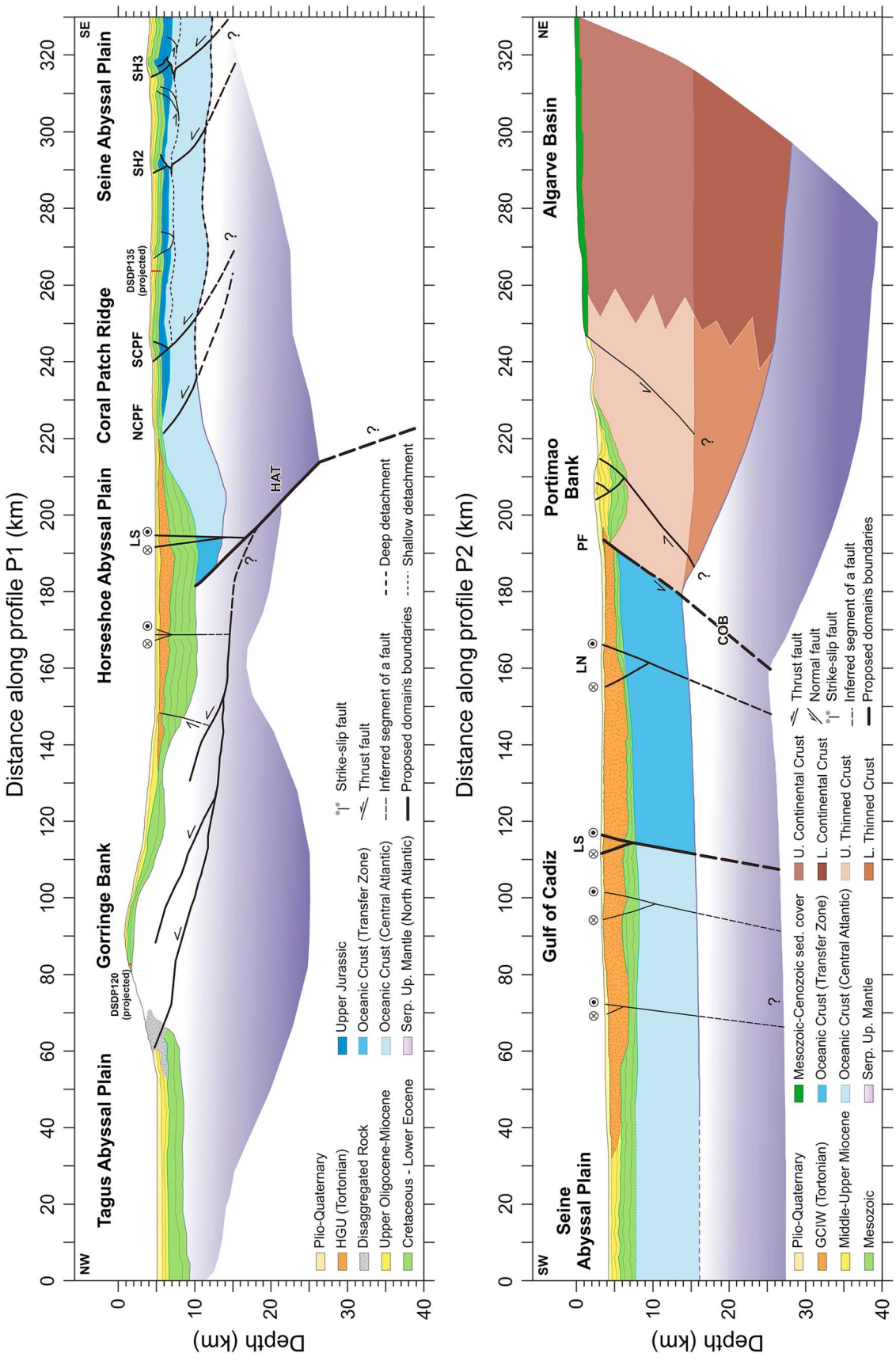

Figure 8. (a) Regional tectonic and stratigraphic synthetic cross section along profile P1, from the Tagus Abyssal Plain to the Seine Abyssal Plain. DSDP Site 120 [*Ryan et al.*, 1973] and Site 135 [*Hayes et al.*, 1972] are located. (b) Regional tectonic and stratigraphic synthetic cross section along profile P2, from the South Portuguese margin to the Seine Abyssal Plain. COB: continental-ocean boundary; HAT: Horseshoe Abyssal plain Thrust; LN: Lineament North; LS: Lineament South; NCP: North Coral Patch fault; PF: Portimao Fault; SCP: South Coral Patch fault; SH (2, 3): Seine Hills faults.

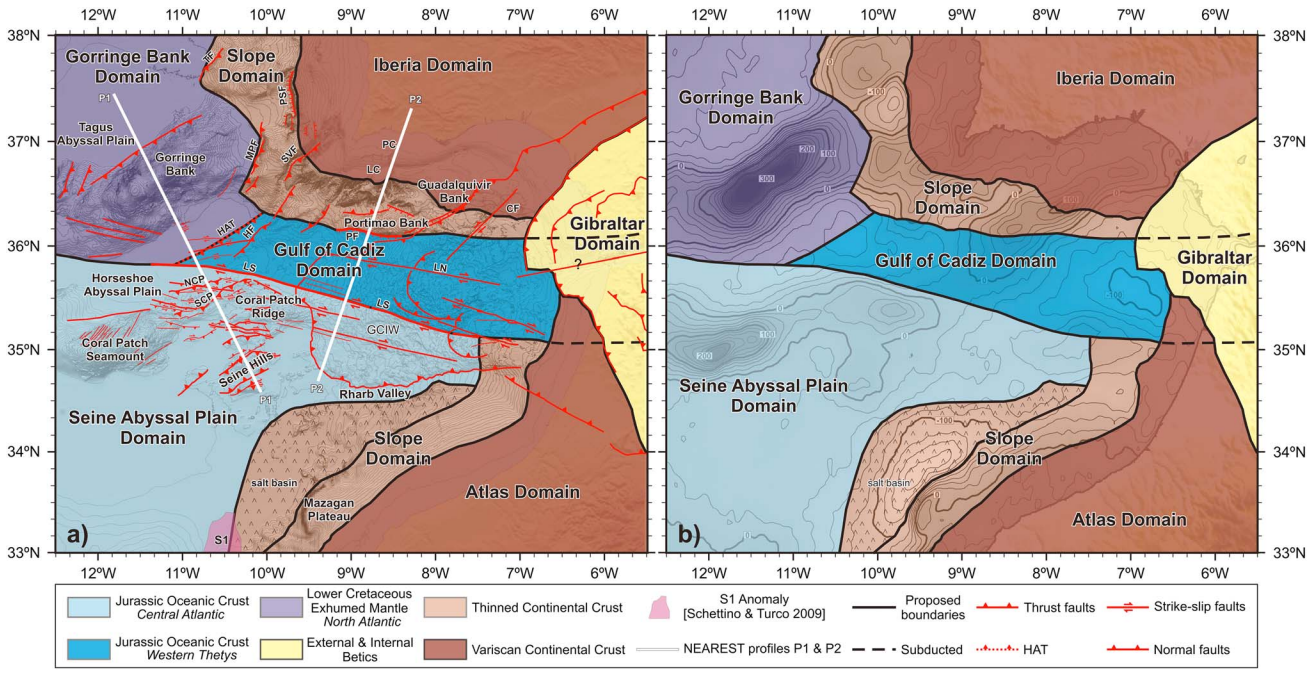

Figure 9. Basement-affinity distribution map (i.e., geological domains) of the SW Iberian margin overlaid by (a) the bathymetric map from the SWIM compilation [*Zitellini et al*., 2009] and GEBCO digital atlas (http://www.gebco.net/) with the main tectonic structures of the region [after *Iribarren et al*., 2009; *Zitellini et al*., 2009; *Bartolome et al*., 2012; *Martínez-Loriente et al*., 2013]. White lines labeled P1 and P2 correspond to the WAS profiles acquired during the NEAREST-SEIS survey [*Sallarès et al*., 2011, 2013]. Purple band displays magnetic anomaly S1 [e.g., *Schettino and Turco*, 2009]; and (b) the free-air anomaly map (contours each 100 mGal) [*Sandwell and Smith*, 1997]. Seven geological domains, defined on the basis of nature of the basement and age, have been proposed. See text for explanation. CF: Cadiz Fault; GCIW: Gulf of Cadiz imbricated wedge; HAT: Horseshoe Abyssal plain Thrust; HF: Horseshoe Fault; LC: Lagos Canyon; LN: Lineament North; LS: Lineament South; MPF: Marquês de Pombal Fault; NCP: North Coral Patch Ridge Fault; PC: Portimão Canyon; PF: Portimão Fault; PSF: Pereira de Sousa Fault; SCP: South Coral Patch Ridge Fault; SVF: São Vicente Fault.

and Turco, 2009; *Sallarès et al*., 2013]. Later, the Neogene NW-SE convergence between Eurasia and Africa resulted in the thrusting of the southeastern segment of the band over the northwestern part, a process that generated the uplift of the Gorringe Bank [*Sallarès et al*., 2013] (Figure 8a). The velocity and gravity modeling of this part of profile P1 reveals a low-velocity/high-serpentinization anomaly, which is possibly related to the presence of a main basal detachment thrust fault with secondary thrusts responsible of the Gorringe Bank uplift (Figure 8a). Moreover, low velocities in the upper part of the basement (Figure 3) indicate a high degree of fracturing and/or serpentinization in the NW flank of the Gorringe Bank, leading eventually to rock disaggregation [*Sallarès et al*., 2013], which added to a steeper slope and may favor large mass-transport deposits [e.g., *Gràcia et al*., 2010; *Lo Iacono et al*., 2012] (Figure 8a).

The boundary between the exhumed mantle rocks flooring the NW part of the profile P1 and the oceanic crust of the SE half occurs beneath the center of the Horseshoe Abyssal Plain. We suggest that the transition between both basement types is abrupt and the HAT appears to be a likely candidate to accommodate the boundary between them (Figures 7, 8a, and 9). The oceanic crust basement of the Coral Patch Ridge and Seine Abyssal Plain must be intensely fractured and highly heterogeneous, displaying local anomalies that may represent ultramafic rock fragments generated by an ultraslow-spreading center (Figures 8a and 9). Although the basement was not reached by DSDP Site 135, on the basis of sediment rates the deduced age of the sediments lying directly above the basement would be 180–155 Ma (Early to Late Jurassic) [*Hayes et al*., 1972]. Kinematic reconstructions differ in the age of the onset of seafloor spreading in the Central Atlantic Ocean (CAO). Some works propose a late Early Jurassic to early Middle Jurassic (185 Ma to 175 Ma), in particular for the northern part of the CAO [*Withjack et al*., 1998; *Roeser et al*., 2002; *Schettino and Turco*, 2009], whereas other authors proposed an age as early as Early Jurassic (195 Ma to 185 Ma) [*Laville et al*., 1995; *Olsen*, 1997; *Le Roy and Piqué*, 2001; *Sahabi et al*., 2004; *Labails et al*., 2010]. On the basis of the end of salt deposition off Morocco and Nova Scotia, *Sahabi et al*. [2004] proposed an age of Late Sinemurian (190 Ma) for the first oceanic crust in the CAO. This age is in agreement with that of the volcanic activity on both sides of the Atlantic ocean referred to as the Central Atlantic Magmatic Province (200 Ma, before the end of salt deposits)

[*Jourdan et al*., 2009]. *Labails et al*. [2010] proposed that during the initial breakup and the first 20 Ma of seafloor spreading (190–170 Ma) ocean accretion was very slow (i.e., a full spreading rate of 8 mm/yr). This spreading rate is within the range of ultraslow accretion, and under these conditions the generation of thin oceanic crust with the presence of localized exhumed mantle rock fragments, as suggested for the Coral Patch Ridge and Seine Hills areas, would be plausible. In addition, *Labails et al*. [2010] proposed that a marked change in the relative plate motion direction (from NNW-SSE to NW-SE) and in the spreading rate (increasing to full spreading rate of 17 mm/yr) took place in the early Bajocian (170 Ma). Given the counterclockwise rotation of Africa and Iberia relative to Eurasia since Early Cretaceous time, the spreading center which would have generated this oceanic crust initially would have to be oriented ~ ENE-WSW or E-W (i.e., the relative plate motion direction would be ~ NNW-SSE), in agreement with the ~ ENE-WSW present-day alignment of the oceanic crust tilted blocks located in the Coral Patch Ridge and Seine Hills areas [*Martínez-Loriente et al*., 2013]. Considering all these elements, we suggest that the oceanic crust present in the SE half of profile P1 would have been generated during the early, slow-to-ultraslow phase of seafloor spreading of the NE segment of the Central Atlantic ridge (starting between 190 and 180 Ma, i.e., Lower Jurassic).

Although not as evident as in profile P2 [*Sallarès et al*., 2011], the location of crustal-scale, SE dipping low-velocity anomalies identified in the Coral Patch Ridge and Seine Abyssal Plain affecting from the sedimentary cover to the first kilometers below the Moho coincide reasonably well with the large, active faults recently identified in these areas [*Martínez-Loriente et al*., 2013] (Figures 3 and 8a). These major thrust faults affect old, cold, and brittle oceanic lithosphere and probably root in a common detachment layer located either at the Moho (~7–8 km below the seafloor) or below the serpentinized area in the uppermost mantle (~12–13 km below the seafloor) [*Martínez-Loriente et al*., 2013] (Figure 8a). This last hypothesis is the one that better agrees with the low velocity of the uppermost mantle, which might be indicative of serpentinization, possibly enhanced by fluid percolation along the thrust faults.

Seismic stratigraphy suggests that most of the regional uplift occurred between the Early and Late Miocene [e.g., *Hayes et al*., 1972; *Sartori et al*., 1994; *Tortella et al*., 1997], consistent with the emplacement of the Horseshoe Gravitational Unit, a large allochthonous body that fills the Horseshoe Abyssal Plain and acts as a regional marker [e.g., *Sartori et al*., 1994; *Torelli et al*., 1997; *Iribarren et al*., 2007; *Martínez-Loriente et al*., 2013] (Figure 8a). MCS data also reveal active deformation in the sedimentary sequence infilling the Horseshoe Abyssal Plain mainly due to WNW-ESE dextral strike-slip faults, which correspond to the westward continuation of the SWIM faults [e.g., *Rosas et al*., 2009, 2012; *Terrinha et al*., 2009; *Zitellini et al*., 2009; *Bartolome et al*., 2012; *Martínez-Loriente et al*., 2013] (Figure 8a). The low-velocity anomaly identified in the sedimentary sequence beneath OBS 19 (~212 km) (Figure 3) spatially coincides with the location of Lineament South (LS), the most prominent of these strike-slip faults [e.g., *Bartolome et al*., 2012; *Martínez-Loriente et al*., 2013].

5.2.2. Geological Cross Section Along Profile P2: From the South Portuguese Margin to the Seine Abyssal Plain

The profile P2, which runs from the Portuguese continental shelf to the Seine Abyssal Plain across the central Gulf of Cadiz, reveals the presence of three main crustal domains [*Sallarès et al*., 2011] (Figures 1 and 8b): to the north a section corresponding to the ~30 km thick Variscan continental crust, then a ~60 km wide transition zone where most of the crustal thinning concentrates, and finally a 150 km wide portion with a ~7 km thick of oceanic crust (Figure 8b).

According with the new information provided by the profile P1, integrated with previous WAS data results [*Gutscher et al*., 2002; *Contrucci et al*., 2004; *Jaffal et al*., 2009] and taking into account recent kinematic reconstructions [e.g., *Stampfli et al*., 2002; *Sahabi et al*., 2004; *Schettino and Turco*, 2009; *Labails et al*., 2010], we suggest that the 150 km long southern part of profile P2 might be actually composed of two oceanic crust segments generated at different oceanic spreading systems (Figure 8b). The northern part (~80 km wide, from ~110 to 190 km along profile P2) would correspond to the remnant of the western Alpine-Tethys crust, generated by oblique seafloor spreading trough a large transform fault boundary between Iberia and Africa during the Jurassic (180–145 Ma), as initially proposed by *Sallarès et al*. [2011]. The southern part (~110 km wide, from 0 to 110 km along profile P2) would correspond to a crust generated during the first stages of seafloor spreading of the NE segment of the Central Atlantic in the Early Jurassic. This is the same spreading center that formed the oceanic crust of the Coral Patch Ridge and Seine Abyssal Plain interpreted in profile P1 (Figures 8 and 9).

The velocity model along profile P2 shows a number of south dipping low-velocity anomalies that have been proposed to represent crustal-scale faults [*Sallarès et al*., 2011], as previously identified in the area from MCS profiles [e.g., *Gràcia et al*., 2003b; *Iribarren et al*., 2007; *Rosas et al*., 2009; *Terrinha et al*., 2009; *Zitellini et al*., 2009; *Bartolome et al*., 2012]. Some of them may correspond to reactivated inherited structures from the Jurassic transfer zone [*Terrinha et al*., 2009; *Zitellini et al*., 2009; *Duarte et al*., 2011; *Sallarès et al*., 2011 *Martínez-Loriente et al*., 2013]. Based on its location, regional relevance, and geometry, we suggest that the largest and bathymetrically most prominent of these crustal-scale faults, LS, is a likely candidate to represent the boundary between both oceanic crustal domains (i.e., the Alpine-Tethys and the Central Atlantic). In this case, LS could be interpreted as the present-day expression of the Gibraltar Fault (GiF), a paleo-plate boundary located between Iberia and Morocco at ~150 Ma [e.g., *Schettino and Turco*, 2009].

Regarding the sedimentary sequence and according to previous interpretations of MCS data [e.g., *Tortella et al*., 1997; *Maldonado et al*., 1999; *Gràcia et al*., 2003b; *Iribarren et al*., 2007], the lower layer corresponds to the well-consolidated Mesozoic sequence, whereas the upper ones corresponds to the GCIW and the Plio-Quaternary sediments (Figure 8b). Toward the north, the Portimão Bank sequence consists of Mesozoic to Plio-Quaternary folded and faulted sediments [e.g., *Gràcia et al*., 2003b; *Terrinha et al*., 2009]. In between these two domains, the Portimão Fault (PF) may correspond to the COT. In the northernmost 100 km of profile P2, the continental basement is overlain by a thin Mesozoic and Cenozoic sedimentary cover [e.g., *Oliveira et al*., 1992] (Figures 8b and 9).

5.2.3. Geological Domains of the SW Iberian Margin

The map of basement affinities of the SW Iberian margin includes seven different geological domains, four of continental affinity: the Iberia, the Atlas, the Gibraltar Arc, and the Slope, and three oceanic: the Gulf of Cadiz, the Seine Abyssal Plain, and the Gorringe Bank (Figure 9).

The Iberia and Atlas domains are constituted mainly by Variscan continental crust [e.g., *Saadi et al*., 1985; *Oliveira et al*., 1992; *Frizon de Lamotte et al*., 2009; *Rodríguez-Fernández*, 2004]. Both continental domains are bounded by the Slope domain, a band made of thinned continental crust. This transition between the Continental and Slope domains is clearly displayed in the northern part of profile P2 (Figure 8b), which agrees with the structure observed along the onshore IBERSEIS WAS transect [*Palomeras et al*., 2008]. It is also consistent with that of *González et al*. [1996], which is based on land recordings of the IAM data (Figure 1). The adjoining Gibraltar Arc domain is composed of the Betics and Rif cordilleras and the Alboran Basin [e.g., *Comas et al*., 1999].

In the Moroccan margin, the Slope domain leads to a salt basin to the west [*Labails et al*., 2010], which is clearly identifiable in the free-air gravity map (Figure 9b). The S1 magnetic anomaly (Figures 1 and 9a) marks the location of the COB in this area. The Seine Abyssal Plain domain includes the Jurassic oceanic crust generated during the Central Atlantic Opening and extends through the western Horseshoe Abyssal Plain, the Coral Patch Ridge, the Seine Abyssal Plain, and the southern part of the central Gulf of Cadiz. Figure 9a shows that the structural pattern in the Seine domain is predominantly characterized by NE-SW thrust faults. Seismic velocities in this basement domain are rather heterogeneous, and the igneous oceanic crust (i.e., L3) is remarkably thin (Figures 3 and 8a). This oceanic crust has been imaged in a number of WAS profiles acquired during different cruises, for instance in the western part of SISMAR profile SIS-P16 [*Gutscher et al*., 2002] and in the southern part of NEAREST profile P2 (Figure 1) [*Sallarès et al*., 2011]. Further south, oceanic crust was interpreted in two other SISMAR profiles, although there the crustal thickness is rather variable ranging from ~7 km in Profile SIS-P4 [*Contrucci et al*., 2004] to 4–6 km in profile SIS-P5 [*Jaffal et al*., 2009] and 3.5–6 km along the NEAREST-SEIS profile P1 in the Coral Patch Ridge and Seine Hills areas (Figure 1). The S1 magnetic anomaly, which is the northernmost segment of the West Africa Coast Magnetic Anomaly, the African conjugate of the East Coast Magnetic Anomaly [e.g., *Sahabi et al*., 2004; *Schettino and Turco*, 2009], coincides with the continental-ocean crust transition proposed by *Contrucci et al*. [2004] and *Jaffal et al*. [2009] (Figure 9).

According to our interpretation, the major structure LS acts as a boundary between the Seine Abyssal Plain domain and the two adjacent domains to the north: the Gulf of Cadiz and the Gorringe Bank (Figure 9). The Gulf of Cadiz domain is composed of the westernmost part—and the only remnant—of the Jurassic oceanic crust generated during the Alpine-Tethys opening [*Sallarès et al*., 2011]. The eastern segment of this band was probably subducted underneath the Gibraltar Domain during Miocene times [e.g., *Lonergan and White*, 1997],

although some authors consider that this subduction is still active [e.g., *Gutscher et al*., 2002]. As Figure 9a shows, the Gulf of Cadiz domain is characterized by the presence of a set of WNW-ESE strike-slip faults (the SWIM faults) [e.g., *Zitellini et al*., 2009; *Sallarès et al*., 2011]. The ~7 km thick oceanic crust of this domain is clearly imaged in profile P2 (Figure 8b). The Gorringe Bank domain extends from the northern Horseshoe Abyssal Plain, crosses the Gorringe Bank, and includes the southern Tagus Abyssal Plain. It is underlain by Cretaceous exhumed mantle rocks as suggested along the WAS profile P1 [*Sallarès et al*., 2013] (Figures 3 and 8a) and evidenced by available rock samples from the drilling Site DSDP 120 [*Ryan et al*., 1973]. The HAT, the structure newly identified in this work, is the limit between the Gulf of Cadiz and Gorringe Bank domains (Figure 9). Even if more data are needed to corroborate this hypothesis, it is possible that this structure was oriented NE-SW, following the trend of the main earthquake cluster located in the middle of the Horseshoe Abyssal Plain and west of the Horseshoe Fault, which could in turn explain the moment tensor solutions of reverse faulting of earthquakes occurring at a depth of 40–60 km that have been described in the area [e.g., *Stich et al*., 2006, 2010; *Geissler et al*., 2010] (Figures 1 and 9).

5.3. Geodynamic Evolution of the SW Iberian Margin

In this section we suggest a framework for the geodynamic evolution of the study area since the breakup of Pangaea until the present day, integrating previously existing and these new data and observations. Thus, Figure 10 includes the six most representative stages of the geodynamic evolution of the SW Iberian margin as well as neighboring areas. To accomplish this goal, we have considered previous kinematic reconstructions proposed by different authors [e.g., *Stampfli et al*., 2002; *Sahabi et al*., 2004; *Labails et al*., 2010; *Schettino and Turco*, 2011] that we have modified introducing the new findings and elements proposed in this work.

In the Late Triassic the rift systems that cut Pangaea from the Caribbean to the Tethys were established. These systems included rift structures in the eastern North America [e.g., *Schlische et al*., 2002], south Iberia [e.g., *Martin-Rojas et al*., 2009], northwest Africa [e.g., *Le Roy and Piqué*, 2001], western Morocco [e.g., *Piqué and Laville*, 1995], and the Atlas [*Schettino and Turco*, 2009, and references therein]. As stated before, seafloor spreading in the CAO started around 190 Ma with a full spreading rate of ~8 mm/yr during the first 20 Ma [e.g., *Olsen*, 1997; *Le Roy and Piqué*, 2001; *Sahabi et al*., 2004; *Schettino and Turco*, 2009; *Labails et al*., 2010]. The rifting in the Atlas region continued during this interval, but structures at the northern boundary of Morocco became more important, separating this plate from Iberia and Newfoundland. Figure 10a summarizes the situation at ~183 Ma, when the first oceanic crust was generated in the CAO and in the incipient Alpine-Tethys system (Ligurian Basin, LB), and the activity of the rift structures in the Atlas region were close to end [*Schettino and Turco*, 2009].

Once the extension in the Atlas region ceased, the Atlantic kinematics was transferred to the Alpine-Tethys domain through the Gibraltar Fault (GiF), a preexisting plate boundary between Iberia and Morocco. This transform margin later evolved into an oblique seafloor spreading system that opened a narrow oceanic basin separating southern Iberia from NW Africa [*Stampfli et al*., 2002; *Schettino and Turco*, 2009; *Sallarès et al*., 2011] (Figure 10b). At this time the SW Iberian margin was underlain by the oceanic crusts that now constitute the Seine Abyssal Plain and the Gulf of Cadiz domains, which were generated by two different oceanic spreading systems that functioned simultaneously: the Central Atlantic and the Alpine-Tethys ones (Figure 10b). From that moment on, the Moroccan plate remained fixed to NW Africa [*Schettino and Turco*, 2009].

Between chrons M22 (~150 Ma) and M21 (147.7 Ma) took place the northward shift of the Atlantic-Tethys transfer zone to the North Pyrenean Fault Zone, through where will be transferred the Atlantic plate kinematics to the east [*Schettino and Turco*, 2009]. As a result of this event, the spreading center of the Alpine-Tethys system stopped at the SW Iberian margin and rifting started between North America and Iberia [*Tucholke et al*., 2007]. During this earliest phase of the North Atlantic opening (147–133 Ma) the southernmost and older part of the ZECM that conforms the Gorringe Bank domain was generated. According with the ages of the Gorringe Bank rock samples [*Féraud et al*., 1986, 1996], the continental mantle denudation progressed northward along the West Iberian margin during the Early Cretaceous (until ~122 Ma) generating the ZECM of the Iberia Abyssal Plain (Figure 10c).

At ~120 Ma took place an important change of relative plate motions between Eurasia, North America, and Africa. The North Atlantic rifting caused the counterclockwise rotation of Iberia with respect to Eurasia and

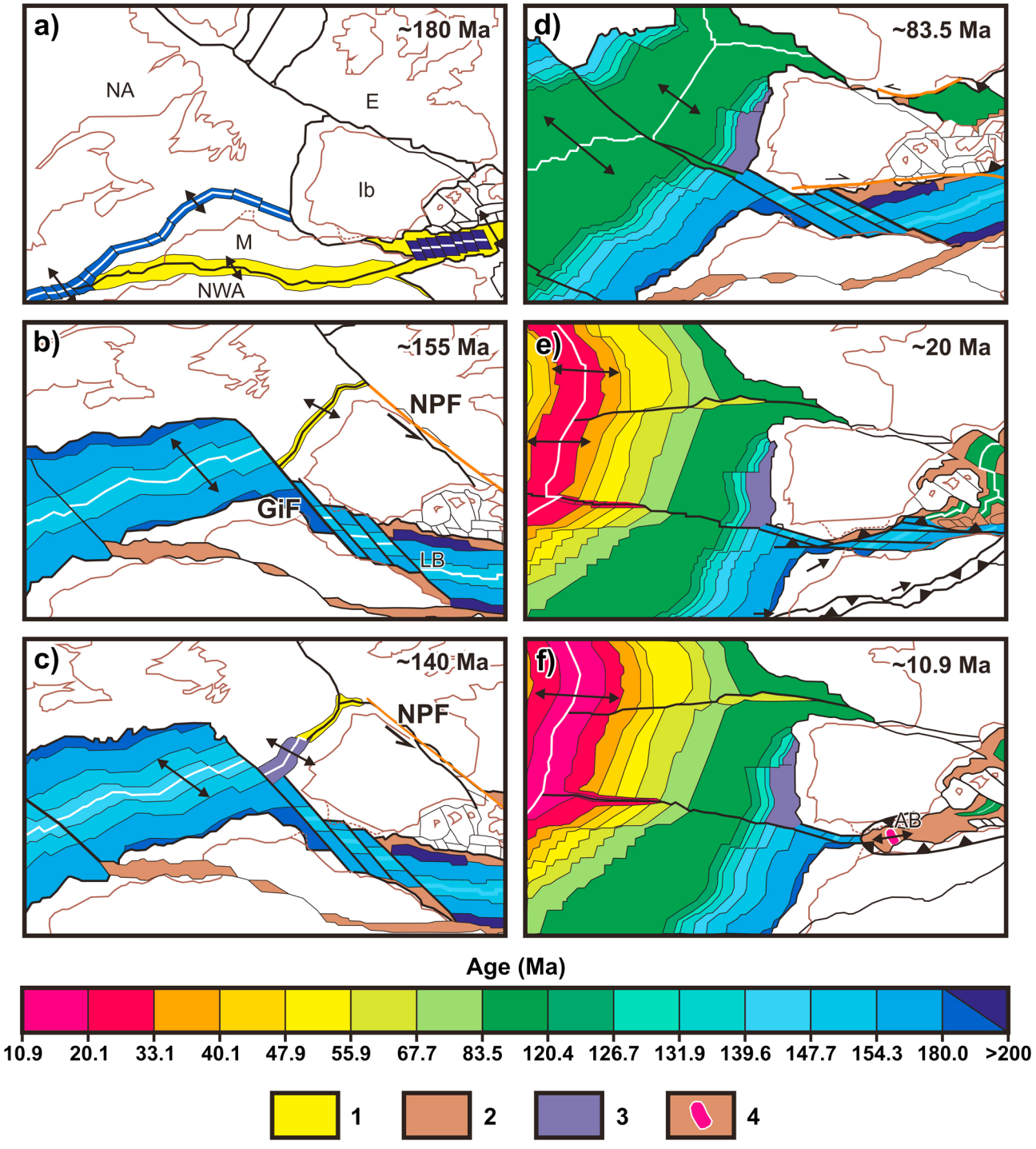

Figure 10. Sketch of the kinematic evolution of the African, Iberian, Eurasian, and American plates at the following stages: (a) 180 Ma, (b) 155 Ma, (c) 140 Ma, (d) 83.5 Ma, (e) 20 Ma, and (f) 10.9 Ma. The kinematic evolution is based primarily on *Schettino and Turco* [2011], although other works [e.g.. *Stampfli et al.*, 2002; *Sahabi et al.*, 2004; *Booth-Rea et al.*, 2007; *Labails et al.*, 2010; *Schettino and Turco* 2009] have also been used to better constrain all the observations. AB: Alboran Basin; E: Eurasia; GiF: Gibraltar Fault; Ib: Iberia; LB: Ligurian Basin; M: Morocco; NPF: North Pyrenean Fault Zone; NA: North America; NWA: northwest Africa; (1) areas affected by active rifting and thinning; (2) areas with thinned crust; (3) exhumed mantle rocks; (4) active volcanic arc; transform faults are shown in orange. White lines are spreading centers.

Africa, triggering the opening of the Bay of Biscay [*Sibuet et al.*, 2004, and references therein]. At 83.5 Ma a convergent boundary between Eurasia and Iberia was formed, beginning the early Pyrenean orogeny [*Sibuet et al.*, 2004], the stopping of the Bay of Biscay spreading center, and the inactivity of the transform boundary between Iberia and Morocco [*Schettino and Turco*, 2009] (Figure 10d).

At the beginning of the Cenozoic, the convergence at the Pyrenees ceased temporarily until Eocene times, when it was reactivated with very slow convergence rates that continued until chron C13n (33.1 Ma) [*Schettino and Turco*, 2009]. The convergence between Africa and Eurasia was accommodated along the southern and eastern margins of Iberia. Then, the Pyrenean belt ceased to be a major plate boundary and Iberia remained fixed to Eurasia onward [*Schettino and Turco*, 2009]. During this period, a subduction zone developed in the southern margin of Iberia where the Alpine-Tethys oceanic lithosphere began to be consumed [*Schettino and Turco*, 2009]. In the Atlantic Ocean, a ridge-ridge-transform triple junction was formed. The higher spreading rates of the southern ridge induced the eastward escape of the Moroccan block with respect to northwest Africa [*Schettino and Turco*, 2009], and the Triassic-Jurassic rift structures of the Atlas were reactivated as reverse faults, uplifting the mountain range [*Beauchamp et al*., 1999; *Frizon de Lamotte et al*., 2000; *Piqué et al*., 2002] (Figure 10e). At ~19 Ma (chron C6n, Early Burdigalian) the Atlas uplift and the Alpine-Tethys oceanic spreading in the western Mediterranean ended [*Schettino and Turco*, 2009]. At ~10.9 Ma (chron C5, early Tortonian), the westward migration of the subduction front due to a process of slab rollback generated the Alboran back-arc basin, and large allochtonous units and gravitational accumulations were emplaced in the Gulf of Cadiz [e.g., *Lonergan and White*, 1997] (Figure 10f). In the SW Iberian margin the NW-SE trending plate convergence produced the reactivation of the WNW-ESE structures generated by the Jurassic transfer zone of the Alpine-Tethys system, the large majority of them concentrated in the Gulf of Cadiz domain. Moreover, the series of NE-SW thrust structures described in Figure 8 and located in the Gorringe and Seine domains, such as the reverse fault responsible of the overthrusting and uplifting of the Gorringe Bank, were developed during that time (Figure 9).

6. Conclusions

Combined WAS and gravity modeling along the SE part of NEAREST-SEIS profile P1 reveals the presence of a thin oceanic crust beneath the sedimentary layer in the Coral Patch Ridge and Seine Abyssal Plain. The velocity structure is characterized by the presence of a thinner-than-normal oceanic layer L3 (0.5–3 km thick), a high lateral variability with low- and high-velocity anomalies, and a discontinuous Moho. The high-velocity anomalies coincide with the places where PmP reflections were not identified. The presence of ultramafic rock fragments in the thin L3 could explain both the high velocities and the lack of PmPs. This velocity structure is comparable to that described in oceanic crust generated at ultraslow-spreading centers. The SE dipping low-velocity anomalies may be the tomographic expression of fault-related rock fracturing, which may favor rock alteration by fluid percolation. The uppermost mantle shows low velocities that may be indicative of mantle serpentinization at the upper mantle levels, suggesting that the thrust faults identified in the MCS profiles cross the Moho and root at the upper mantle.

According with kinematic reconstructions, we propose that the oceanic crust present in the Coral Patch Ridge and Seine Abyssal Plain areas was generated during the early, slow (~8 mm/yr) stages of seafloor spreading of the NE segment of the Central Atlantic, 190–180 Ma. There is evidence in the WAS data for the presence of a sharp limit in the middle of the Horseshoe Abyssal Plain between an oceanic crust and the exhumed mantle rocks interpreted in the NW part of the plain. The transition might take place trough the HAT, a deep SE dipping reflector with a dip angle of ~30°. This newly identified structure may be associated with the seismicity cluster located in the middle of the Horseshoe Abyssal Plain, which shows moment tensor solutions of reverse faulting at depths of 40–60 km.

After a reassessment of the profile P2, which runs from the south Portuguese margin to the Seine Abyssal Plain, and considering kinematic reconstructions, we propose that the 150 km wide segment of oceanic crust is actually composed of two different segments generated by different rift systems. The northern part (~80 km wide) would correspond to the only remnant western Alpine-Tethys generated by oblique seafloor spreading trough a transform system that developed between Iberia and Africa at Early-Late Jurassic (180–145 Ma), whereas the southern segment would have been generated during the first stages of seafloor spreading of the Central Atlantic. These two domains are separated by the LS strike-slip fault, the longest of the inherited structures from the Jurassic transform zone that were reactivated during the Neogene convergence.

According with the new basement affinities interpreted based on the NEAREST-SEIS profiles and integrating previous results from other WAS and MCS data, rock basement samples, and location of magnetic anomalies, we propose that the basement offshore the SW Iberian margin is composed of three main oceanic domains: (1) the Seine Abyssal Plain domain, made of oceanic crust generated in the NE Central Atlantic during Early Jurassic and characterized by a NE-SW trending tectonic architecture inherited from the initial oceanic spreading; (2) the Gulf of Cadiz domain, made of oceanic crust generated in the Alpine-Tethys system, coeval with the formation of the Seine Abyssal Plain domain, and characterized by the presence of a set of WNW-ESE strike-slip faults (the SWIM faults) that are inherited structures from oblique rifting between Iberia and Morocco; and (3) the Gorringe Bank domain, made of exhumed mantle rocks and generated during the first stages of North Atlantic opening, just after the end of spreading between Iberia and Africa. The complex and large diversity of basement types flooring the SW Iberian margin must shed a new light into the characterization of the seismogenic and tsunamigenic sources in the region. Consequently, from now on, the geological variability between domains revealed by our findings (i.e., age, lithology, and rheology) will need to be taken into account in any further seismic and tsunami hazard assessment models of the SW Iberian margin.

Acknowledgments

We thank the captain, crew, and scientific and UTM-CSIC and IFREMER technical staff onboard the R/V *Hespérides* during the NEAREST-SEIS cruise. The NEAREST project has been funded by the EU Programme "Integrating and Strengthening the European Research Area" of FP6, Sub-Priority 1.1.6.3, "Global Change and Ecosystems," contract 037110, and the NEAREST-SEIS survey was funded by the Complementary Action CGL2006-27098-E/ BTE of the Spanish MICINN. Additional support came from the MICINN projects MEDOC (CTM2007-66179-C02-02/MAR), POSEIDON (CTM2010-21569), EVENT (CGL2006-12861-C02-02), ESF TopoEurope TOPOMED project (CGL2008-03474-E/BTE), SHAKE (CGL2011-30005-C02-02), and COST Action ES1301 "FLOWS." We also acknowledge funding from MICINN through the Ramon y Cajal programme (R. Bartolome) and CSIC that funded the JAE-Pre fellowship of S. Martínez-Loriente. We thank Editor A. Revil and reviewers J. Duarte and T. Minshull for helpful suggestions and comments. This work was carried out within the Grups de Recerca de la Generalitat de Catalunya B-CSI (2009 SGR 146).

References

Auffret, Y., P. Pelleau, F. Klingelhoefer, L. Geli, J. Crozon, J. Y. Lin, and J. C. Sibuet (2004), MicrOBS: A new generation of ocean bottom seismometer, *First Break*, *22*(7), 41–47.

Auzende, J. M., et al. (1984), Intraoceanic tectonism on the Gorringe Bank: Observations by submersible, in *Ophiolites and Oceanic Lithosphere*, Geol. Soc. Spec. Publ., vol. 13, edited by I. G. Gass, S. J. Lippard, and A. W. Shelton, pp. 113–120, Geological Society of London, London.

Baldy, P., G. Boillot, P. A. Dupeuble, J. Malod, I. Moita, and D. Mougenot (1977), Carte geólogique du plateau continental Sud-Portugais et Sud-Espagnol (Golfe de Cadix), *Bull. Geol. Soc. Fr.*, *XIX*, 703–724.

Banda, E., M. Torne, and the IAM Group (1995), Iberian Atlantic margins group investigates deep structure of ocean margins, a multichannel seismic survey, *EOS*, *76*(3), 25–29.

Bartolome, R., E. Gràcia, D. Stich, S. Martinez-Loriente, D. Klaeschen, F. L. Mancilla, C. Lo Iacono, J. J. Dañobeitia, and N. Zitellini (2012), Evidence for active strike-slip faulting along the Eurasia-Africa convergence zone: Implications for seismic hazard in the SW Iberian Margin, *Geology*, *40*(6), 495–498, doi:10.1130/G33107.1.

Beauchamp, W., R. W. Allmendinger, M. Barazangi, A. Demnati, M. El Alji, and M. Dahmani (1999), Inversion tectonics and the evolution of the High Atlas Mountains, Morocco, based on a geological-geophysical transect, *Tectonics*, *18*, 163–184, doi:10.1029/1998TC900015.

Booth-Rea, G., C. R. Ranero, J. M. Martínez-Martínez, and I. Grevemeyer (2007), Crustal types and Tertiary tectonic evolution of the Alborán sea, western Mediterranean, *Geochem. Geophys. Geosyst.*, *8*, Q10005, doi:10.1029/2007GC001639.

Buforn, E., M. Bezzeghoud, A. Udias, and C. Pro (2004), Seismic sources on the Iberia-African plate boundary and their tectonic implications, *Pure Appl. Geophys.*, *161*, 623–646, doi:10.1007/s00024-003-2466-1.

Carlson, R. L., and C. N. Herrick (1990), Densities and porosities in the oceanic crust and their variations with depth and age, *J. Geophys. Res.*, *95*, 9153–9170.

Carlson, R. L., and D. J. Miller (2003), Mantle wedge water contents estimated from seismic velocities in partially serpentinized peridotites, *Geophys. Res. Lett.*, *30*(5), 1250 doi: 10.1029/2002GL016600.

Christensen, N., and W. Mooney (1995), Seismic velocity structure and composition of the continental crust: A global view, *J. Geophys. Res.*, *100*, doi:10.1029/95JB00259.

Comas, M. C., J. P. Platt, J. I. Soto, and A. B. Watts (1999), The origin and tectonic history of the Alboran Basin: Insights from leg 161 results, in *Proc. ODP, Sci. Res*, vol. 161, edited by R. Zahn, M. C. Comas, and A. Klaus, pp. 555–580, Ocean Drilling Program, College Station, TX.

Contrucci, I., F. Klingelhöfer, J. Perrot, R. Bartolome, M. A. Gutscher, M. Sahabi, J. Malod, and J. P. Rehault (2004), The crustal structure of the NW-Moroccan Continental Margin for wide-angle and reflection seismic data, *Geophys. J. Int.*, *159*(1), 117–128, doi:10.1111/j.1365-246X.2004.02391.x.

Dean, S. M., T. A. Minshull, R. B. Whitmarsh, and K. E. Louden (2000), Deep structure of the ocean-continent transition in the southern Iberia abyssal plain from seismic refraction profiles: The IAM-9 transect at 40°20′N, *J. Geophys. Res.*, *105*, 5859–5885.

DeMets, C., R. G. Gordon, and D. F. Argus (2010), Geologically current plate motions, *Geophys. J. Int.*, *181*, 1–80, doi:10.1111/j.1365-246X.2009.04491.x.

Dick, H. J. B., J. Lin, and H. Schouten (2003), An ultraslow-spreading class of ocean ridge, *Nature*, *426*, 405–412, doi:10.1038/nature02128.

Duarte, J. C., F. M. Rosas, P. Terrinha, M.-A. Gutscher, J. Malavieille, S. Silva, and L. Matias (2011), Thrust-wrench interference tectonics in the Gulf of Cadiz (Africa-Iberia plate boundary): Insights from (sand-box) analog models, *Mar. Geol.*, *289*, 135–149.

Féraud, G., D. York, C. Mével, G. Cornen, C. M. Hall, and J. M. Auzende (1986), Additional 40Ar39Ar dating of the basement and the alkaline volcanism of Gorringe Bank (Atlantic Ocean), *Earth Planet. Sci. Lett.*, *79*(3–4), 255–269.

Féraud, G., M. O. Beslier, and G. Cornen (1996), $^{40}Ar/^{39}Ar$ dating of gabbros from the ocean/continent transition of the western Iberia margin: Preliminary results, in *Proceedings of the Ocean Drilling Program, Scientific Results*, vol. 149, edited by R. B. Whitmarsh et al., pp. 489–495, Ocean Drilling Program, College Station, Tex.

Frizon de Lamotte, D., B. Saint Bezar, R. Bracèe, and E. Mercier (2000), The two main steps of the Atlas building and geodynamics of the western Mediterranean, *Tectonics*, *19*, 740–761, doi:10.1029/2000TC900003.

Frizon de Lamotte, D., P. Leturmy, Y. Missenard, S. Khomsi, G. Ruiz, O. Saddiqi, F. Guillocheau, and A. Michard (2009), Mesozoic and Cenozoic vertical movements in the Atlas system (Algeria, Morocco, Tunisia): An overview, *Tectonophysics*, *475*, 9–28, doi:10.1016/j.tecto.2008.10.024.

Fukao, Y. (1973), Thrust faulting at a lithospheric plate boundary, The Portugal earthquake of 1969, *Earth Planet Sci. Lett.*, *18*, 205–216.

Fullea, J., J. C. Afonso, M. Fernàndez, J. Vergés, and H. Zeyen (2010), The structure and evolution of the lithosphere–asthenosphere boundary beneath the trans-Mediterranean region, *Lithos*, *120*, 74–95, doi:10.1016/j.lithos.2010.03.003.

Geissler, W. H., et al. (2010), Focal mechanisms for sub-crustal earthquakes in the Gulf of Cadiz from dense OBS deployment, *Geophys. Res. Lett.*, *37*, L18309, doi:10.1029/2010GL044289.

Girardeau, J., G. Cornen, M. O. Beslier, B. Le Gall, C. Monnier, P. Agrinier, G. Dubuisson, L. Pinheiro, A. Ribeiro, and A. Whitechurch (1998), Extensional tectonics in the Gorringe Bank Rocks, eastern Atlantic Ocean: Evidence of an oceanic ultra-slow mantellic accreting centre, *Terra Nova*, *10*(6), 330–336.

González, A., M. Torné, D. Córdoba, N. Vidal, L. M. Matias, and J. Díaz (1996), Crustal thinning in the southwestern Iberia margin, *Geophys. Res. Lett.*, *23*, 2477–2480.

González, A., D. Córdoba, R. Vegas, and L. M. Matias (1998), Seismic crustal structure in the southwest of the Iberian Peninsula and the Gulf of Cadiz, *Tectonophysics*, *296*, 317–331, doi:10.1016/S0040-1951(98)00151-6.

Gràcia, E., J. J. Dañobeitia, J. Vergés, and PARSIFALTeam (2003a), Mapping active faults offshore Portugal (36°N–38°N): Implications for seismic hazard assessment along the southwest Iberian margin, *Geology*, *31*, 83–86.

Gràcia, E., J. J. Danobeitia, J. Verges, and R. Bartolome (2003b), Crustal architecture and tectonic evolution of the Gulf of Cadiz (SW Iberian margin) at the convergence of the Eurasian and African plates, *Tectonics*, *22*(4), 1033, doi:10.1029/2001TC901045.

Gràcia, E., A. Vizcaino, C. Escutia, A. Asioli, A. Rodés, R. Pallàs, J. Garcia Orellana, S. Lebreiro, and C. Goldfinger (2010), Holocene earthquake record offshore Portugal (SW Iberia): Testing turbidite paleoseismology in a slow-convergence margin, *Quat. Sci. Rev.*, *29*, 1156–1172.

Gutscher, M. A., J. Malod, J. P. Rehault, I. Contrucci, F. Klingelhoefer, L. Mendes-Victor, and W. Spakman (2002), Evidence for active subduction beneath Gibraltar, *Geology*, *30*, 1071–1074.

Hamilton, E. L. (1978), Sound velocity-density relations in sea-floor sediments and rocks, *J. Acoust. Soc. Am.*, *63*, 366–377.

Hayes, D. E., et al. (1972), *Site 135. Initial Reports of the Deep Sea Drilling Project*, vol. 14, pp. 15–48, U.S. Government Printing Office, Washington, D. C.

Hayward, N., A. B. Watts, G. K. Westbrook, and J. S. Collier (1999), A seismic reflection and GLORIA study of compressional deformation in the Gorringe Bank region, eastern North Atlantic, *Geophys. J. Int.*, *138*(3), 831–850.

Hinz, K., E. L. J. Winterer, and S. S. Party (1984), *Initial Reports DSDP 79*, vol. 79, U.S. Government Printing Office, Washington, D. C.

Iribarren, L., J. Vergés, F. Camurri, J. Fullea, and M. Fernàndez (2007), The structure of the Atlantic-Mediterranean transition zone from the Alboran Sea to the Horseshoe Abyssal Plain (Iberia–Africa plate boundary), *Mar. Geol.*, *243*, 97–119.

Iribarren, L., J. Verges, and M. Fernandez (2009), Sediment supply from the Betic-Rif orogeny to basins through Neogene, in *The Geology of Vertical Movements of the Lithosphere*, Tectonophysics, vol. 475, edited by G. Bertotti et al., pp. 68–84, doi:10.1016/j.tecto.2008.11.029.

Jaffal, M., F. Klingelhoefer, L. Matias, F. Teixeira, and M. Amrhar (2009), Crustal structure of the NW Moroccan margin from deep seismic data (SISMAR cruise), *Geoscience*, *341*(6), 495–503, doi:10.1016/j.crte.2009.04.003.

Jiménez-Munt, I., M. Fernàndez, J. Vergés, J. C. Afonso, D. Garcia-Castellanos, and J. Fullea (2010), Lithospheric structure of the Gorringe Bank: Insights into its origin and tectonic evolution, *Tectonics*, *29*, TC5019, doi:10.1029/2009TC002458.

Johnston, A. (1996), Seismic moment assessment of earthquakes in stable continental regions—III New Madrid 1811–1812, Charleston 1886 and Lisbon 1755, *Geophys. J. Int.*, *126*, 314–344.

Jourdan, F., A. Marzoli, H. Bertrand, S. Cirilli, L. H. Tanner, D. J. Kontak, G. McHone, R. P. Renne, and G. Bellieni (2009), 40Ar/39Ar ages of CAMP in North America: Implications for the Triassic–Jurassic boundary and the 40 K decay constant bias, *Lithos*, *110*, 167–180.

Kern, H., and J. M. Tubia (1993), Pressure and temperature dependence of *P*- and *S*-wave velocities, seismic anisotropy and density of sheared rocks from the sierra alpujata massif (Ronda peridotites, southern Spain), *Earth Planet. Sci. Lett.*, *119*(1–2), 191–205.

Korenaga, J., W. S. Holbrook, G. M. Kent, P. B. Kelemen, R. S. Detrick, H.-C. Larsen, J. R. Hopper, and T. Dahl-Jensen (2000), Crustal structure of the southeast Greenland margin from joint refraction and reflection seismic tomography, *J. Geophys. Res.*, *105*, 21,591–21,614, doi:10.1029/2000JB900188.

Korenaga, J., W. S. Holbrook, R. S. Detrick, and P. B. Kelemen (2001), Gravity anomalies and crustal structure at the southeast Greenland margin, *J. Gophys. Res.*, *106*, 8853–8870.

Labails, C., J. L. Olivet, D. Aslanian, and W. R. Roest (2010), An alterantive early opening scenario for the Central Atlantic Ocean, *Earth Planet. Sci. Lett.*, *297*(3–4), 355–368, doi:10.1016/j.epsl.2010.06.024.

Lanaja, J. M., A. Navarro, J. L. Martínez Abad, J. DelValle, L. M. Rios, J. Plaza, R. del Potro, and J. Rodríguez de Pedro (1987), *Contribución de la Exploración Petrolífera al Conocimiento de la Geología de España*, pp. 465, Inst. Geol. y Min. de España, Madrid.

Laville, E., A. Charroud, B. Fedan, M. Charroud, and A. Piqué (1995), Inversion négative et rifting atlasique: Le bassin triasique de Kerrouchkne (Moyen Atlas, Maroc), *Bull. Soc. Geol. Fr.*, *116*, 364–374.

Le Roy, P., and A. Piqué (2001), Triassic–Liassic western Moroccan synrift basins in relation to the central Atlantic opening, *Mar. Geol.*, *172*, 359–381, doi:10.1016/S0025-3227(00)00130-4.

Lo Iacono, C., et al. (2012), Large, deep water slope failures: Implications for landslide generated tsunamis, *Geology*, *40*(10), 931–934.

Lonergan, L., and N. White (1997), Origin of the Betic-Rif Mountain belt, *Tectonics*, *16*, 504–522, doi:10.1029/96TC03937.

Maldonado, A., L. Somoza, and L. Pallarés (1999), The Betic orogen and the Iberian-African boundary in the Gulf of Cádiz: Geological evolution (central North Atlantic), *Mar. Geol.*, *155*, 9–43.

Malod, J. A., and D. Mougenot (1979), L'histoire géologique néogène du Golfe de Cadix, *Bull. Soc. Geol. Fr.*, *XXI*, 603–611.

Martínez-Loriente, S., et al. (2013), Active deformation in old oceanic lithosphere and significance for earthquake hazard: Seismic imaging of the Coral Patch Ridge area and neighboring abyssal plains (SW Iberian Margin), *Geochem. Geophys. Geosyst.*, *14*, 2206–2231, doi: 10.1002/ggge.20173.

Martin-Rojas, I., R. Somma, F. Delgado, A. Estévez, A. Iannace, V. Perrone, and V. Zamparelli (2009), Triassic continental rifting of Pangaea: Direct evidence from the Alpujarride carbonates, Betic Cordillera, SE Spain, *J. Geol. Soc. London*, *166*(3), 447–458, doi:10.1144/0016-76492008-091.

Medialdea, T., R. Vegas, L. Somoza, J. T. Vázquez, A. Maldonado, V. Díaz-del-Río, A. Maestro, D. Córdoba, and M. C. Fernández-Puga (2004), Structure and evolution of the "Olistostrome" complex of the Gibraltar Arc in the Gulf of Cadiz (eastern Central Atlantic): Evidence from two long seismic cross-sections, *Mar. Geol.*, *209*(1–4), 173–198.

Miller, D. J., and N. I. Christensen (1997), Seismic velocities of lower crustal and upper mantle rocks from the slow-spreading Mid-Atlantic Ridge, south of the Kane Transform (MARK), *Proc. Ocean Drill. Program Sci. Results*, *153*, 437–454.

Minshull, T. A., M. R. Muller, and R. S. White (2006), Crustal structure of the southwest Indian ridge at 66°E: Seismic constraints, *Geophys. J. Int.*, *166*(1), 135–147.

Moser, T. J., G. Nolet, and R. Snieder (1992), Ray bending revisited, *Bull. Seismol. Soc. Am.*, *82*(1), 259–288.

Muller, M. R., T. A. Minshull, and R. S. White (2000), Crustal structure of the southwest Indian ridge at the Atlantis II fracture zone, *J. Geophys. Res.*, *105*, 25,809–25,828.

Nocquet, J. M., and E. Calais (2004), Geodetic measurements of crustal deformation in the Western Mediterranean and Europe, *Pure Appl. Geophys.*, *161*, 661–681.

Oliveira, T., et al. (1992), Carta Geológica de Portugal, escala 1: 500.000, (coord. T. Oliveira), Serviços Geológicos de Portugal.

Olsen, P. E. (1997), Stratigraphic record of the early Mesozoic breakup of Pangea in the Laurasia-Gondwana rift system, *Annu. Rev. Earth Planet. Sci.*, *25*, 337–401.

Palomeras, I., R. Carbonell, I. Flecha, F. Simancas, P. Ayarza, J. Matas, D. Martinez-Poyatos, A. Azor, F. González-Lodeiro, and A. Pérez-Estaún (2008), The nature of the lithosphere across the Variscan Orogen of SW-Iberia: Dense wide-angle seismic reflection data, *J. Geophys. Res.*, *114*, B02302, doi:10.1029/2007JB005050.

Parker, R. L. (1974), A new method for modeling marine gravity and magnetic anomalies, *J. Geophys. Res.*, *79*(14), 2014–2016, doi:10.1029/JB079i014p0201.

Pinheiro, L. M., R. B. Whitmarsh, and P. R. Miles (1992), The ocean-continent boundary off the western continental margin of Iberia-II. Crustal structure in the Tagus Abyssal Plain, *Geophys. J. Int.*, *109*, 106–124.

Piqué, A., and E. Laville (1995), L'ouverture initiale de l'Atlantique Central, *Bull. Soc. Geol. Fr.*, *166*, 725–738.

Piqué, A., P. Tricart, R. Guiraud, E. Laville, S. Bouaziz, M. Amrhar, and R. A. Ouali (2002), The Mesozoic–Cenozoic Atlas belt (North Africa): An overview, *Geodinamica Acta*, *15*, 185–208, doi:10.1016/S0985-3111(02)01088-4.

Purdy, G. M. (1975), The eastern end of the Azores-Gibraltar plate boundary, *Geophys. J. R. Astron. Soc.*, *43*, 123–150.

Rodríguez-Fernández, L. R. (2004), Mapa Tectónico de España 1:2.000.000, in *Geología de España*, edited by J. A. Vera, pp. 69–72, SGE-IGME, Madrid.

Roeser, H. A., C. Steiner, B. Schreckenberger, and M. Block (2002), Structural development of the Jurassic Magnetic Quiet Zone off Morocco and identification of Middle Jurassic magnetic lineations, *J. Geophys. Res.*, *107*(B10), 2207, doi:10.1029/2000JB000094.

Rosas, F. M., J. C. Duarte, P. Terrinha, V. Valadares, and L. Matias (2009), Morphotectonic characterization of major bathymetric lineaments in Gulf of Cadiz (Africa–Iberia plate boundary): Insights from analogue modeling experiments, *Mar. Geol.*, *261*(1–4), 33–47, doi:10.1016/j.margeo.2008.08.002.

Rosas, F. M., J. C. Duarte, M. C. Neves, P. Terrinha, S. Silva, and L. Matias (2012), Thrust-wrench interference between major active faults in the Gulf of Cadiz (Africa-Eurasia plate boundary, offshore SW Iberia): Tectonic implications from analogue and numerical modeling, *Tectonophysics*, *548–549*, 1–21.

Rovere, M., C. R. Ranero, R. Sartori, L. Torelli, and N. Zitellini (2004), Seismic images and magnetic signature of Late Jurassic to Early Cretaceous Africa-Eurasia plate boundary off SW Iberia, *Geophys. J. Int.*, *158*, 554–568.

Ryan, W. B. R., K. J. Hsü, M. B. Cita, P. Dumitrica, J. Lort, W. Maync, W. D. Nesteroff, G. Pautot, H. Stradner, and F. C. Wezel (1973), Site 120, in *Initial Reports of the Deep Sea Drilling Project*, vol. XIII, edited by A. G. Kaneps, pp. 19–41, US Gov. Printing Office, Washington, D. C.

Saadi, M., E. A. Hilali, M. Bensaïd, A. Boudda, and M. Dahmani (1985), Carte Géologique du Maroc 1:1.000.000. Ministère de l'Énergie et des Mines, Direction de la Géologie, *Editions du Service Géologique du Maroc*.

Sahabi, M., D. Aslanian, and J. L. Olivet (2004), A new starting point for the history of the central Atlantic, *C. R. Geosci.*, *336*, 1041–1052.

Sallarès, V., and C. R. Ranero (2005), Structure and tectonics of the erosional convergent margin off Antofagasta, north Chile (23_300S), *J. Geophys. Res.*, *110*, B06101, doi:10.1029/2004JB003418.

Sallarès, V., J. J. Danobeitia, and E. R. Flueh (2000), Seismic tomography with local earthquakes in Costa Rica, *Tectonophysics*, *329*(1), 61–78, doi:10.1016/S0040-1951(00)00188-8.

Sallarès, V., Ph. Charvis, E. R. Flueh, J. Bialas, and the SALIERI Scientific Party (2005), Seismic structure of the Carnegie ridge and the nature of the Galápagos hotspot, *Geophys. J. Int.*, *161*, 763–788, doi:10.1111/j.1365-246X.2005.02592.x.

Sallarès, V., A. Gailler, M. A. Gutscher, D. Graindorge, R. Bartolome, E. Gràcia, J. Díaz, J. J. Dañobeitia, and N. Zitellini (2011), Seismic evidence for the presence of Jurassic oceanic crust in the central Gulf of Cadiz (SW Iberia margin), *Earth Planet. Sci. Lett.*, *311*, 112–123, doi:10.1016/j.epsl.2011.09.003.

Sallarès, V., S. Martínez-Loriente, M. Prada, E. Gràcia, C. R. Ranero, M. A. Gutscher, R. Bartolome, A. Gailler, J. J. Dañobeitia, and N. Zitellini (2013), Seismic evidence of exhumed mantle rock basement at the Gorringe Bank and the adjacent Horseshoe and Tagus abyssal plains (SW Iberia), *Earth Planet. Sci. Lett.*, *365*, 120–131, doi:10.1016/j.epsl.2013.01.021.

Sandwell, D. T., and W. H. F. Smith (1997), Marine gravity anomaly from geosat and ERS 1 satellite altimetry, *J. Geophys. Res.*, *102*, 10,039–10,054.

Sandwell, D. T., and W. H. F. Smith (2009), Global marine gravity from retracked Geosat and ERS-1 altimetry: Ridge segmentation versus spreading rate, *J. Geophys. Res.*, *114*, B01411, doi:10.1029/2008JB006008.

Sartori, R., L. Torelli, N. Zitellini, D. Peis, and E. Lodolo (1994), Eastern segment of the Azores-Gibraltar line (central-eastern Atlantic): An oceanic plate boundary with diffuse compressional deformation, *Geology*, *22*, 555–558.

Schettino, A., and E. Turco (2009), Breakup of Pangaea and plate kinematics of the central Atlantic and Atlas regions, *Geophys. J. Int.*, *178*, 1078–1097.

Schettino, A., and E. Turco (2011), Tectonic history of the western Tethys since the Late Triassic, *Geol. Soc. Am. Bull.*, *123*(1-2), 89–105, doi:10.1130/B30064.1.

Schlische, R. W., M. O. Withjack, and P. E. Olsen (2002), Relative timing of CAMP, rifting, continental breakup, and inversion: Tectonic significance, in *The Central Atlantic Magmatic Province: Insights From Fragments of Pangea*, Geophysical Monograph, vol. 136, edited by W. E. Hames et al., pp. 33–59, AGU, Washington, D. C.

Sibuet, J.-C., S. P. Srivastava, and W. Spakman (2004), Pyrenean orogeny and plate kinematics, *J. Geophys. Res.*, *109*, B08104, doi: 10.1029/2003JB002514.

Srivastava, S. P., H. Schouten, W. R. Roest, K. D. Klitgord, L. C. Kovacs, J. Verhoef, and R. Macnab (1990), Iberian plate kinematics: A jumping plate boundary between Eurasia and Africa, *Nature*, *344*, 756–759.

Srivastava, S. P., J. C. Sibuet, S. Cande, W. R. Roest, and I. D. Reid (2000), Magnetic evidence for slow seafloor spreading during the formation of the Newfoundland and Iberian margins, *Earth Planet. Sci. Lett.*, *182*(1), 61–76.

Stampfli, G. M., G. D. Borel, R. Marchant, and J. Mosar (2002), A plate tectonic model for the Paleozoic and Mesozoic, *Earth Planet. Sci. Lett.*, *196*(1–2), 17–33.

Stich, D., E. Serpelloni, F. Mancilla, and J. Morales (2006), Kinematics of the Iberia–Maghreb plate contact from seismic moment tensors and GPS observations, *Tectonophysics*, *426*, 295–317.

Stich, D., R. Martin, and J. Morales (2010), Moment tensor inversion for Iberia-Maghreb earthquakes 2005–2008, *Tectonophysics*, *483*, 390–398, doi:10.1016/j.tecto.2009.11.006.

Tarantola, A. (1987), *Inverse Problem Theory: Methods for Data Fitting and Model Parameter Estimation*, pp. 613, Elsevier Science, New York.

Terrinha, P., et al. (2009), Morphotectonics and strain partitioning at the Iberia–Africa plate boundary from multibeam and seismic reflection data, *Mar. Geol.*, *267*, 156–174.

Thiebot, E., and M. A. Gutscher (2006), The Gibraltar Arc seismogenic zone (part 1): Constraints on a shallow east dipping fault plane source for the 1755 Lisbon earthquake provided by seismic data, gravity and thermal modeling, *Tectonophysics*, *426*, 135–152, doi:10.1016/j.tecto.2006.02.024.

Toomey, D. R., and G. R. Foulger (1989), Tomographic inversion of local earthquake data from Hengill-Grensdalur central volcano complex, Iceland, *J. Geophys. Res.*, *94*, 17,497–17,510.

Torelli, L., R. Sartori, and N. Zitellini (1997), The giant chaotic body in the Atlantic Ocean off Gibraltar: New results from a deep seismic reflection survey, *Mar. Pet. Geol.*, *14*, 125–138.

Tortella, D., M. Torne, and A. Perez-Estaun (1997), Geodynamic evolution of the eastern segment of the Azores–Gibraltar Zone: The Gorringe Bank and Gulf of Cadiz region, *Mar. Geophys. Res.*, *19*, 211–230.

Tucholke, B. E., D. S. Sawyer, and J. C. Sibuet (2007), Breakup of the Newfoundland-Iberia Rift, in *Imaging, Mapping, and Modelling Continental Lithosphere Extension and Breakup*, *Geol. Soc.*, Spec. Pub, vol. 282, edited by G. D. Karner, G. Manatschal, and L. M. Pinheiro, pp. 9–46, Geological Society of London, London.

White, R. S., D. McKenzie, and R. K. O'Nions (1992), Oceanic crustal thickness from seismic measurements and rare earth element inversions, *J. Geophys. Res.*, *97*, 19,683–19,715.

Whitmarsh, R. B., G. Manatschal, and T. A. Minshull (2001), Evolution of magma-poor continental margins from rifting to seafloor spreading, *Nature*, *413*(6852), 150–154.

Withjack, M. O., R. W. Schlische, and P. E. Olsen (1998), Diachronous rifting, drifting, and inversion on the passive margin of central eastern North America; an analog for other passive margins, *AAPG Bull.*, *82*, 817–835.

Zitellini, N., M. Rovere, P. Terrinha, F. Chierici, L. Matias, and BIGSETS Team (2004), Neogene through Quaternary tectonic reactivation of SW Iberian Passive Margin, *Pure Appl. Geophys.*, *161*, 565–587.

Zitellini, N., et al. (2009), The quest for the Africa-Eurasia plate boundary west of the Strait of Gibraltar, *Earth Planet. Sci. Lett.*, *280*, 13–50, doi:10.1016/j.epsl.2008.12.005.